Block Detection and European Heat Waves

Master's Thesis

Faculty of Sciences

University of Bern

presented by

LEONIE VILLIGER

2017

Supervisor:

Prof. Dr. Olivia Romppainen-Martius

Institute of Geography, Mobiliar Lab for Natural Risks and

Oeschger Centre for Climate Change Research

University of Bern

Advisors:

Sina Lenggenhager and Matthias Röthlisberger

Institute of Geography and

Oeschger Centre for Climate Change Research

University of Bern

Abstract

Heat waves, which threaten society and endanger human health, can be related to atmospheric blocks. These blocks, often defined as stationary high-pressure systems within the latitudes of the westerlies, are able to block the westerly flow, resulting in prolonged periods of clear-sky conditions. Various methods for identifying blocks exist, and they can be grouped into two categories: (1) detecting an anticyclonic flow anomaly, and (2) detecting the meridional reversal of the flow. The resulting blocking climatologies vary substantially, which may lead to inconsistent conclusions regarding the effect of blocks on heat waves. In this master's thesis, five block-detection indices are compared using ERA-interim data from 1979 to 2015. Besides the comparison of the two detection categories, comparisons between different variables and different intensity thresholds are conducted. Four focal points are investigated: (1) The northern hemispheric summer blocks of the five indices are compared, leading to the conclusion that the indices' blocks vary substantially regarding their number, location, size, and lifetime. (2) Three intensity thresholds are assigned to the corresponding percentiles of the extratropical field anomalies, revealing that the thresholds extract between 3% and 14% of the field anomalies. Furthermore, it is shown that the thresholds directly determine the range of latitudes at which blocks can be detected. (3) A number of European heat wave case studies are analysed, showing that only in one of seven cases do the indices agree on the presence of a block. Moreover, the case studies reveal that two indices erroneously detect subtropical high-pressure systems. (4) The interaction of blocks and heat waves in several European regions is addressed. Here it is shown that for northern regions the indices detect the blocks at the same location and that all indices' blocks increase the odds for a heat wave by a factor of 10, while for southern regions the indices do not agree on the location of the blocks nor on the change of the odds for a heat wave.

Contents

1 Introduction

Heat waves pose a serious threat to society. The extreme temperatures afflict human health critically. Alone the European heat wave in 2003 caused around 70'000 fatalities (ROBINE et al. 2008). In addition, heat waves are often accompanied by continuing drought conditions that can lead to crop failure and devastating fires. Heat waves are associated with stationary weather conditions that are often interpreted as atmospheric blocks (e.g. TRIGO et al. 2005, YAMADA et al. 2016). Therefore, it is important to study blocks and their relation to heat waves.

A block is characterized by a quasi-stationary anticyclone within the latitudes of the westerlies (e.g. BLUESTEIN 1993, BUEHLER et al. 2011). The quasi-stationary anticyclone contributes to the development of heat through three different processes: (1) The anticyclonic rotation transports warm air from low to mid-latitudes (e.g. TRIGO et al. 2004, DOLE et al. 2011). (2) The subsidence in the centre of the anticyclone leads to clear sky conditions and hence to an anomalous surface radiation budget that heats the air diabatically. (3) Simultaneously, adiabatic heating takes place when the descending air masses are compressed (BIELI et al. 2015). Not only circulation anomalies, but also the soil moisture content influence surface temperatures (e.g. BLACK et al. 2004, PERKINS 2015).

Two different views on the definition of a block exist in the scientific community. Either the block contains the anticyclone itself or the meridional overturning of the zonal flow, i.e. the equatorward edge of the anticyclone, is interpreted as the block. It is important to note that anticyclones accompanied by a cyclone (Figure 1.i-iii) to the south always cause an overturning of the flow; while ridges (Figure 1.iii) represent anticyclones but do not necessarily cause an overturning of the flow. Therefore, a stationary, high-amplitude ridge can either be interpreted as block or not.

This debate is reflected in the definition of different blocking indices. Blocking indices are needed for objectively detecting blocks. On the one hand, reversal indices, which are effective in detecting dipole and omega blocks, exist. On the other hand, anomaly based indices, which detect dipole and omega blocks, but also stationary, high-amplitude ridges, exist. Furthermore, blocking indices differ due to

the used variable, like, e.g., geopotential height (GPH) or potential vorticity (PV), and due to various criteria relating to the duration, the stationarity, and the minimum size of a block.

The ambiguity regarding the detection of blocks brings up the question how strongly the detected features differ between various blocking indices. Moreover, it is questionable whether the relation between blocks and heat waves is dependent on the blocking index or not. In this master's thesis, five blocking indices are compared within the frame of European heat waves. In a first step, the characteristics of each index's blocks are assessed with the following questions: *Where on the northern hemisphere are the blocking indices detecting blocks during summer? What are the differences between the indices' summer blocking frequency? Can these differences be explained in relation to the number, duration and size of the blocks?*

A lot of research has been done on the impact of blocks on heat waves. PFAHL and WERNLI (2012), for example, used the anomaly-based index by SCHWIERZ et al. (2004), testing two different intensity thresholds, -1.3 and -0.7 pvu. They found that with a first threshold, 80% of the blocks coincide with heat waves, while, with a second threshold, this applies for only for 50%. Therefore, in a second step, the effect of the threshold choice for the SCHWIERZ et al. (2004) index is analysed by answering the following questions: *What percentile are -1.3, -1.0, and -0.7 pvu representing in the extratropical summer distribution of the anomalous, vertically-averaged potential vorticity (APV')? What fraction of the APV' values per latitude that fall below a threshold are classified as blocks?*

For case studies on heat waves associated with blocks (e.g. SCHNEIDEREIT et al. 2012, TRIGO et al. 2005) the definition of a block is a critical issue. An illustrative example is the European heat wave in 2003: While TRIGO et al. (2005) interpreted the synoptic situation during this event as a block, SOUSA et al. (2017) pointed out that the term block is wrongly used in this particular case. In the context of this debate, in a third step, a number of European heat waves are studied to compare the five blocking indices by addressing the subsequent questions: *Which of the blocking indices are detecting a block during the selected European heat events? Where are the blocking indices positioned relative to each other and relative to the heat index during the selected European heat events?*

Recently, BRUNNER et al. (2017) found that, in the spring season, heat waves in northern Europe are associated with increased blocking activity in the same region, while heat waves in the south are associated with decreased blocking activity in the north. Similar findings for the summer season were made by SOUSA et al. (2017), who concluded that high-latitude blocks are associated with positive temperature anomalies in Scandinavia and negative temperature anomalies in southern Europe. These

studies raise the question of whether the same spatial relation between blocks and heat are found, if different blocking indices are used. Therefore, in a fourth step, the spatial block-heat relation is analysed for three of the blocking indices by addressing the following questions: *How often (relative to the summer climatology) is each grid point blocked when a European heat day occurs? How does the occurrence of a block change the odds for a European heat day? What is the difference between the blocking episodes of the* SCHWIERZ *et al. (2004) index (with an intensity threshold of -1.0 pvu) that are associated with western European heat days and those that are not?*

In Chapter 2 the current state of knowledge and some theoretical background are given. In Chapter 3 the data, the blocking indices, the heat indices, and the methods for each of the four focal points are presented. In Chapter 4 the results are shown and discussed for each of the focal point individually. Finally, the conclusions are drawn in Chapter 5.

2 | Literature Review

2.1 Definition and Properties

In the mid-twentieth century the term blocking or block was introduced for atmospheric features that temporarily block the normal eastward propagation of extratropical cyclones by replacing the zonal flow with a meridional-type flow (ELLIOTT and SMITH 1949, REX 1950). Even though the blocking definition is a matter of ongoing debate, BARRIOPEDRO et al. (2010) summarized some general characteristics of blocks:

(1) A block consists of a large-scale high-pressure system with an anticyclonic rotation in the troposphere, located at the latitudes of the westerlies, and persisting for between several days and five weeks. (2) The blocking high-pressure system is accompanied by one or two low-pressure systems to the south. (3) There are two preferred blocking regions at the exit zone of the main storm tracks, the eastern Pacific and the eastern Atlantic. (4) The blocking frequencies are highest in winter and spring. (5) The blocking frequencies are influenced by teleconnection-patterns, like the North Atlantic Oscillation. (6) Blocks are related to anomalous weather conditions.

Not all authors agree on point (2), the need for a low-pressure system to be associated with the blocking high-pressure system. For instance, BLUESTEIN (1993) defined three blocking patterns, of which the third one is not related to a low-pressure system: the dipole block (also called Rex or high-over-low block), the omega block, and the stationary, high-amplitude ridge (Figure 1).

Recently, SOUSA et al. (2017) emphasized that the term block is being misused for features corresponding to stationary, high-amplitude ridges. They argue that a distinction between high-latitude blocks (dipole and omega blocks) and stationary, high-amplitude ridges is needed; because the former are associated with low temperatures in southern region, while the latter are related to high temperatures in southern regions.

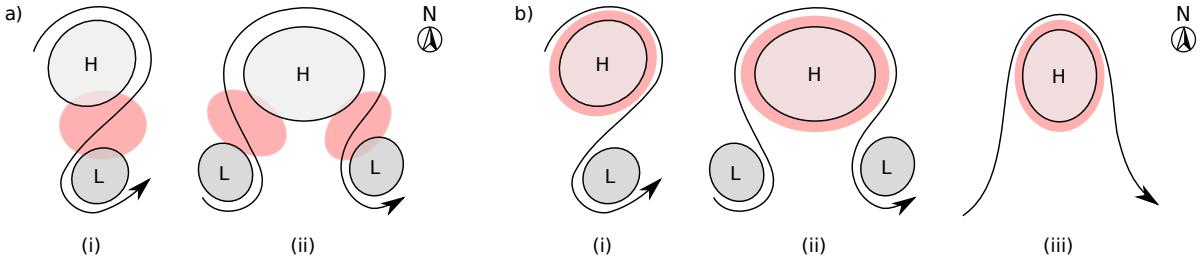

Figure 1: Illustration of the three blocking patterns (i) dipole block, (ii) omega block, (iii) stationary, high-amplitude ridge. Adapted from BLUESTEIN (1993). The letter H stands for highipressure system, the letter L for low-pressure system. The light gray shading denotes negative (positive) PV (GPH) anomalies, the dark gray shading denotes positive (negative) PV (GPH) anomalies. The red shading indicates the regions that are identified as blocks by an index based on a) the reversal of the meridional gradient in the PV or GPH field, b) negative (positive) PV (GPH) anomalies.

2.2 Theories

HOSKINS (1987) and PELLY (2001) summarized some important blocking theories that are briefly presented here. Blocks can be interpreted as the interference of Rossby wave trains in such a way that an amplification of the climatological ridges in the Euro-Atlantic and Pacific region occur (HOSKINS 1987, PELLY 2001). This stationary wave theory is able to explain the location of the blocking frequency maxima (PELLY 2001).

Another global theory is the concept of multiple flow equilibria. This theory proposes two stable states of the atmosphere: a strong zonal flow with low-amplitude waves and a weak zonal flow with high-amplitude waves. In this manner, blocks represent a quasi-stable state of the atmosphere. However, model experiments showed that the existence of multiple equilibria states is questionable (PELLY 2001).

On a local scale, the theory of modons and the theory of solitons are able to explain the maintenance of dipole blocks within a westerly flow. A modon is a localised solution of the quasi-geostrophic equations which describes a vortex pair within a westerly flow. However, modon solutions can only be found under the assumption of a sufficiently large zonal wind speed, which is rarely met in reality. Furthermore, the solutions are not robust for a strong horizontal shear (PELLY 2001).

The theory of solitons is based on a model consisting of the nonlinear, baroclinic quasi-geostrophic potential vorticity equation with a mean zonal wind characterized by a vertical and horizontal shear. MALGUZZI and MALANOTTE-RIZZOLI (1984) showed that solitary Rossby waves that resemble a dipole block can be found in realistic westerly winds.

Blocks can also be studied from an eddy perspective. Multiple studies concluded that eddies help to

maintain a block by transporting anticyclonic vorticity into the blocked region (PELLY 2001). Additionally, one can explain the onset of a block from the eddy perspective: SHUTTS (1983) showed that eddies approaching a split jet can help to form a PV cut-off. This PV cut-off later develops into a block.

The concept of explosive upstream cyclogenesis is another possibility for explaining the onset of blocks. Here, a relation between a fast growing cyclone and a developing block downstream is assumed. This way, blocks are interpreted as the response of the planetary waves to the explosive upstream cyclogenesis (PELLY 2001).

The instability theory was introduced by FREDERIKSEN (1982). FREDERIKSEN (1982) used a two-layer quasi-geostrophic model with three different static stability conditions to study the structure of the fastest growing disturbances. Under the most unstable conditions, a monopole structure grew fastest (cyclogenesis); for less unstable conditions, a dipole structure in the Pacific grew fastest; and for the least unstable conditions, a dipole structure in the Pacific and the Atlantic grew fastest. FREDERIKSEN (1982) interpreted the latter two cases as blocking onsets.

Finally, blocks can be understood from a PV perspective in which a block is an upper-tropospheric negative PV anomaly in the extratropics (e.g. SCHWIERZ et al. 2004, ALTENHOFF et al. 2008, PFAHL et al. 2015). Negative PV anomalies in the extratropics are generated through the polewards transport of subtropical air on an isentropic surface, and/or through the upwards transport from lower-tropospheric air across isentropic surfaces due to diabatic processes (e.g. ALTENHOFF et al. 2008, PFAHL et al. 2015). It is the latent heating within clouds that allows the air to cross the isentropes (PFAHL et al. 2015). ALTENHOFF et al. (2008) found that PV streamers upstream of a block support the two processes and are able to strengthen the block. Later, PFAHL et al. (2015) showed that the two processes are of equal importance.

In the PV framework, the stationarity of a block is explained in terms of the westward flow introduced by a dipole vortex pair that counteracts the eastward jet (Figure 2). Thus, a block consists of a negative PV anomaly polewards of the jet, and one or two positive PV anomalies equatorwards of the jet (ALTENHOFF et al. 2008).

2.3 Detection Methods

BARRIOPEDRO et al. (2010) provides a comprehensive overview of conventional and current block detection methodologies (Figure A1). First of all, a distinction between subjective and objective tech-

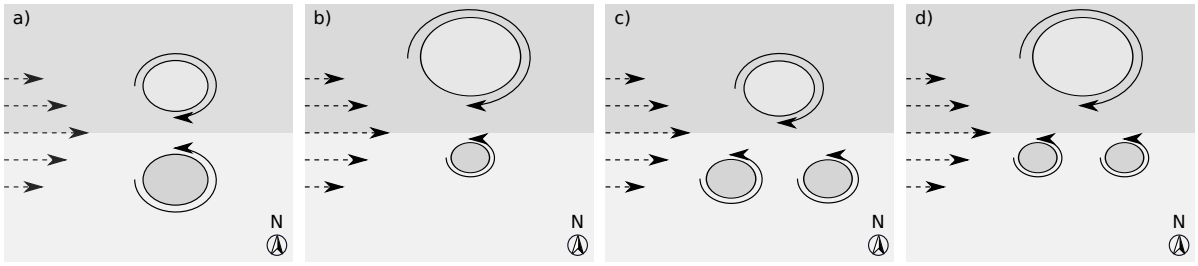

Figure 2: Illustration of highly idealized PV distributions related to a block. The background PV consist of low PV (light shading) equatorwards of the jet (dashed arrows), and high PV (dark shading) polewards of the jet. The blocking anticyclone is shown as a low PV cut-off, and the accompanied cyclones as high PV cut-offs. The winds induced by the PV cut-offs are shown as arrows. Adapted from (ALTENHOFF et al. 2008).

niques is made. REX (1950) visually - therefore subjectively - identified a block as the change from a zonal to a meridional flow. Three decades later, these subjective approaches were replaced by automatic routines, for instance by LEJENÄS and ØKLAND (1983), or TIBALDI and MOLTENI (1990).

Furthermore, the methodologies differ in the variable and the type of field they use to identify the block. Either an absolute field, or a field of anomalies from a reference mean is used. Reversal indices, for instance, scan an absolute field along a given latitude for a reversal of the meridional gradient. By contrast, anomaly-based indices check a field of anomalies on closed contours that are greater or smaller than a certain threshold. Figure 1 illustrates which regions of a given blocking pattern are detected by the two types of indices.

A variety of variables and field-type combinations are used in scientific literature. There are indices detecting the reversal of the meridional GPH gradient (e.g. LEJENÄS and ØKLAND 1983, TIBALDI and MOLTENI 1990); the reversal of the meridional potential temperature gradient (e.g. PELLY and HOSKINS 2003); a positive GPH anomaly (e.g. DOLE and GORDON 1983); or a negative PV anomaly (e.g. SCHWIERZ et al. 2004). Finally, the duration, stationarity, and size criteria applied by an index determine the features that are detected.

One difficulty that arises with the indices detecting the meridional reversal of a gradient is the choice of the reference latitude. A solution for this problem is presented in SCHERRER et al. (2006), who made use of multiple reference-latitudes. For the indices detecting an anomaly, the difficulty lies in choosing an appropriate threshold and reference mean.

In this master's thesis, only one blocking index is investigated that detects the reversal of the meridional GPH gradient. The remaining indices detect an anomaly in the GPH or PV field. The two variables GPH and PV are introduced briefly in the Appendix (Section A.1).

2.4 Relation to Extremes

Blocks can be related to anomalous weather conditions. The stationary anticyclone transports air masses across latitudes, deflects storm tracks, causes subsidence, and leads to long-lasting periods of cloud-free conditions. As a result, high temperatures can be found in the region where the anticyclone causes southerlies, and in the centre of the anticyclone where cloud-free conditions persist (Chapter 1).

In contrast, low temperatures can be found downstream of the anticyclone, in the region where north-easterlies bring cold and dry air from high- to mid-latitudes (SILLMANN et al. 2011). During the transport from high to mid-latitudes the air descends. The descending air is warmed by being compressed. Additionally, the air may be warmed through heat fluxes from the surfaces, if the air moves across the warmer ocean. Therefore, a cold event is dependent on a sufficient cold source region (BIELI et al. 2015). The cloud-free conditions lead to increased outgoing longwave radiation during winter nights which supports the development of low temperatures (SILLMANN et al. 2011). TREIDL et al. (1981) pointed out that in winter a block may cause a temperature inversion near the surface leading to fog or low clouds. Below the temperature inversion low temperatures can develop.

Besides temperature extremes, blocks contribute to precipitation anomalies. On the one hand, a lack of precipitation occurs in the blocked region. On the other hand, remote areas south of the blocking system receive a surplus of precipitation (TRIGO et al. 2004). The reason for this spatial distribution is the deflection of the synoptic systems south and north of the block (SOUSA et al. 2016). Persistent ridges are not accompanied by low pressure systems, and - in contrast to high-latitude blocks - lead to dry conditions in southern regions (SOUSA et al. 2016).

3 | Data and Methods

3.1 Reanalysis Data

Reanalysis data from the ERA-Interim dataset was used. This data product is provided by the European Centre for Medium-Range Weather Forecast. The dataset starts on January 1 1979 and is updated continuously. The product consist of 3-hourly surface parameters containing ocean-wave and land-surface conditions and 6-hourly upper-air parameters. The spatial resolution is approximately 80 km in the horizontal on 60 vertical levels reaching form the surface up to 0.1 hPa height (DEE et al. 2011).

3.2 Blocking Indices

Five different blocking indices were used. The first one is SCHERRER et al. (2006)'s two-dimensional adaptation of TIBALDI and MOLTENI (1990)'s reversal index. The second index defines blocks via positive GPH anomalies. The remaining three indices are variations of SCHWIERZ et al. (2004)'s index based on negative PV anomalies. All five indices have the following criteria in common: a block needs to have a spatial overlap of at least 70% between successive time steps, and needs to persist for at least five successive days.

The output of the five blocking algorithms are 2-dimensional binary fields consisting of blocked and unblocked grid points. While the fields of the first index (TM2D) has a spatial resolution of $2^\circ \times 2^\circ$, the other four indices have a spatial resolution of $1^\circ \times 1^\circ$. A global blocking field is available every six hours for all five indices. Additionally, each block's duration, position and size are available.

3.2.1 TM2D

The first index (TM2D) detects regions with a meridional reversal of the GPH gradient at 500 hPa and follows the procedure by ROHRER et al. (2017). In a first step, the data was remapped onto a $2^\circ \times 2^\circ$

grid. Afterwards, each latitude from 36° to 76°, i.e. 36°, 38°, 40°, etc., was checked for two different GPH gradients, one towards the pole and the other towards the equator. A reversal was identified if the GPH gradient over 14° latitude was smaller than -10 gpm per degree latitude towards the pole and bigger than 0 gpm per degree towards the equator. Finally, the reversed region was labelled as a block if it met the above-stated persistence and stationarity criterion.

3.2.2 RO200

The second index (RO200) detects positive anomalies in the GPH field on 200 hPa. The anomalies were defined with respect to the climatological (1979-2016) 30-day running mean, including the 30 years centred around the actual year (ROHRER 2017a). A block was identified if the anomaly was at least 200 gpm and fulfilled the above-stated persistence and stationarity criteria. This index was proposed by ROHRER (2017a), who empirically justified the threshold of 200 gpm.

3.2.3 SCH13/10/07

The index of SCHWIERZ et al. (2004) detects negative anomalies in the (from 500 hPa to 150 hPa) vertically-averaged PV (APV) field. The anomalies of the APV (APV') field were computed with respect to the climatological (1979-2015) 30-day running mean. All closed contours of the APV' field with values smaller than a certain threshold were selected and labelled as a block if above stated persistence and stationarity criteria were met. The code of the blocking index allows the blocks a maximum lifetime of 180 days.

Originally, SCHWIERZ et al. (2004) set the threshold for the APV' to -1.2 pvu. Here three different thresholds were used, -1.3, -1.0, and -0.7 pvu. Henceforth, this index is referred to with the labels SCH, SCH13, SCH10 or SCH07, according to the threshold applied. Unlike the original index, the index here did not use a minimal size criterion.

3.3 Heat Indices

Two heat indices were used to describe the heat events (Section 4.3) and to identify European heat days (Section 4.4). The first one is the warm spell day index (WSDI) (e.g. BRUNNER et al. 2017) that selects all grid points where the daily mean temperature two meters above ground (T2m) exceeds the daily 90th percentile of the same variable for at least four successive days. The second index, the HUMIDEX, provides information about the sensation of heat by taking into account temperature in

combination with humidity. The spatial resolution for both heat indices is $1^\circ \times 1^\circ$.

3.3.1 Warm Spell Day Index (WSDI)

The 90th percentile of T2m was computed for each grid point and each calendar-day separately. For this the lowest and highest values of T2m during the period from 1979 to 2015 were selected. The 90th percentile was determined from the range given by these two values. So, 366 (one for each day of the year, including leap years) 90th percentile values were assigned to each of the grid points. In a next step, all grid points that showed T2m values greater than the 90th percentile of the corresponding calendar-day were set to one, and all remaining grid points were set to zero.

To check whether the exceedances of the 90th percentiles persisted for at least four days, four successive fields were summed up. All grid points of the summed-up fields that showed a value of four were set to one and all remaining grid points were set to zero. The resulting binary field is the WSDI.

The WSDI was also tested with a duration criterion asking for six (instead of four) consecutive days. However, with a duration criterion of six days only a few, very extreme events were found. As in the case of BRUNNER et al. (2017), no size criterion was used and no coherent area was needed.

The WSDI was computed both with the original T2m and with the detrended T2m. When the original T2m was used, more heat grid points were found in the recent summers compared to the beginning of the ERA-interim period (Section A.2). Here the WSDI based on the detreded T2m was used, because the increasing temperature trend was not the centre of interest. For each grid point the linear trend over the period 1979 to 2015 was computed and subtracted in order to detrend the daily T2m fields.

3.3.2 HUMIDEX

The HUMIDEX is a measure for the heat stress that an average person perceives. It is a combination of temperature and humidity. In other words, it is created by adding a linear function of the vapour pressure to the actual air temperature. The vapour pressure is computed from the dew point temperature. The standard formula provided by the Government of Canada (GOVERNMENT OF CANADA 2017b) is:

$$HUMIDEX = T + \frac{5}{9}(e - 10) = T + \frac{5}{9}(6.11 exp^{5417.7530\left(\frac{1}{273.16} - \frac{1}{Tdew}\right)} - 10) \quad (1)$$

e = vapour pressure (hPa)

T = air temperature (°C)

$Tdew$ = dew point temperature (°K)

T2m was used for T and the dew point temperature two meters above ground was used for $Tdew$. The temperature fields were not detrended to compute the HUMIDEX. The values reported by the HUMIDEX were split up into four ranges which represent the potential hazard of the weather conditions on the human body (GOVERNMENT OF CANADA 2017a):

- 20 to 29: little discomfort
- 30 to 39: some discomfort
- 40 to 45: great discomfort; avoid exertion
- Above 45: dangerous; heat stroke possible

These ranges were used to visualize the heat conditions in the selected heat-wave case studies (Section 4.3).

3.4 Block Characteristics

The blocking frequency was computed for each grid point on the northern hemisphere to assess the spatial distribution of each index's blocks. The blocking frequency is defined as the mean of the binary blocking fields over the selected time period, in this case the months June, July, and August (JJA) from 1979 to 2015. Thus, the frequency value of a grid point describes the percentage of time during which the grid point is blocked.

To explain the differences between the blocking indices' spatial distribution, the number, the size, and the lifetime of the blocks contributing to the blocking frequency were examined. The size of a block was defined as the maximum area that the block reached during its lifetime. All blocks with their centre on the northern hemisphere and occurring in the considered time window were taken into account. The calculation of the area was not possible for 7% (RO200), 3% (SCH13, SCH10), and 1% (SCH07) of the blocks. Possibly, the blocks that reached into the southern hemisphere posed this problem. In any case, these blocks were neglected in the size analysis.

3.5 Threshold Choice

The following steps were conducted to attribute the three thresholds -1.3, -1.0, and -0.7 pvu to a percentile of the extratropical summer APV' distribution: First, all APV' values north of 30°N, during

JJA from 1979 to 2015 were selected. Second, the number of APV' values smaller than each threshold was computed. Third, these counts were weighted with the cosine of the latitude to account for the latitudinal-dependency of each grid point's area. Last, the latitudinally-weighted counts were divided by the sum of the latitudinally-weighted grid points times the number of time steps.

Additionally, the same procedure, although without the latitudinal weighting, was applied for each latitude separately. As a comparison, the mean summer blocking frequencies (Section 3.4) of the three SCH indices were determined for each latitude. Finally, the ratio of the two quantities was computed by dividing the zonally-averaged blocking frequency by the percentage of APV' values per latitude that fall below the corresponding threshold.

3.6 Case Studies

Seven European heat periods were studied. The heat events were found in the scientific literature, but also in reports from national weather services. An overview of the case studies is provided in Table 1. For each case study, all the indices were calculated. Furthermore, the position of the blocking indices relative to each other and relative to the WSDI was investigated. The WSDI and the HUMIDEX were used to assess the severity of the heat event.

Table 1: Case studies listed according to the year and region together with the literature reference.

Year	Region	Reference
1994	Scandinavia	FISCHER et al. (2007) and RUSSO et al. (2015)
2003	Central Europe	MEEHL and TEBALDI (2004) and Z'GRAGGEN (2006)
2006	Central Europe	REBETEZ et al. (2009) and RUSSO et al. (2015)
2007	Greece	KOTRONI et al. (2011) and RUSSO et al. (2015)
2010	Russia	SCHNEIDEREIT et al. (2012) and RUSSO et al. (2015)
2013	British Isles	METOFFICE (2016) and METÉIREANN (2013)
2015	Central Europe	METEOSCHWEIZ (2016) and RUSSO et al. (2015)

Three blocking patterns (Section 2) were used to describe the observed flow situation: (1) dipole block, (2) omega block, and (3) stationary, high-amplitude ridge. The case studies led to the definition of a fourth stationary flow type, a (4) stationary, low-amplitude ridge which is located at low latitudes and does not reach as far north as the blocking pattern (3). The term stationary flow type is used on purpose, because features of type (4) are not considered to be blocks.

3.7 Blocks and Heat

This section focuses on the interaction of blocks and heat waves in a climatological way. First, the fraction fraction of heat waves that is associated with the different blocking indices in several European regions is quantified. Second, it is determined by how much the odds for a heat wave change, given that there is a block.

3.7.1 Definitions

Seven European heat regions (Table 2, Figure 3.a) were defined based on the heat regions identified by STEFANON et al. (2012) (Figure A9). Within each heat region a heat day was defined, if at least 16 grid points reported a warm spell day (WSD). It needs to be mentioned that the heat regions are not equally large, hence the heat days from the different regions are not directly comparable. Before all ocean grid points were masked out, so that only land grid points contributed to the analysis. The number of land grid points within each region are listed in Table 2. As a result, a binary vector (1 = heat day, 0 = no heat day) with 3404 entries (JJA 1979 to 2015) was assigned to each heat region. This heat day definition is adapted from the study of BRUNNER et al. (2017) who asked for at least $5^\circ \times 5^\circ$ WSD grid points within the domain from 35°N to 72.5°N, and 12.5°W to 30°E to define a heat day.

Table 2: Definition of European heat regions based on the heat regions by STEFANON et al. (2012) together with the number of land grid points (LGP), the number of heat days (HD), and the number of heat events (HE) within each heat region. A HD is defined as a day with at least 16 grid point reporting a warm spell day within the heat region. The onset of a HE is found if two HDs are separated more than seven days from each other.

Region	Longitudes [°E]	Latitudes [°N]	LGP	HD	HE
North Sea (NS)	-8 to 15	51 to 62	131	171	38
Scandinavia (SC)	13 to 33	60 to 71	188	178	46
Western Europe (WE)	-3 to 13	43 to 52	138	126	37
Russia (RU)	36 to 45	51 to 63	130	158	38
Eastern Europe (EE)	16 to 31	47 to 59	178	181	55
Iberian Peninsula (IB)	-10 to 3	36 to 44	79	66	21
Southeastern Europe (SE)	26 to 43	35 to 43	106	120	34

3.7.2 Composites

The identified heat days were used to compute the composites of the blocking indices and the GPH at 500 hPa, over the entire European domain (25° W to 50° E, and 35° N to 75° N). Only the blocking indices TM2D, RO200 and SCH10 were considered here. Additionally, the JJA blocking frequencies

were subtracted from the composites to account for the climatology of the blocking indices. In similar way the JJA climatology of the GPH was subtracted from the GPH composites.

To ensure that the composites were not the mean of a single event, it was determined how many different heat events took place in each heat region. The onset of a heat event was identified, if a heat day followed a period of at least seven days without heat (Figure A12). For all seven heat regions the heat days belonged to multiple heat events, distributed over the period from 1979 to 2015.

3.7.3 Odds Ratios

As an additional measure for the block-heat relation, the ratio between heat days with a block and heat days without a block was computed, the so-called odds ratio (OR). It is helpful to introduce the contingency table of the two attributes, heat day and block, before the equation for the OR is shown (Table 3):

Table 3: Contingency table for the two attributes heat day and block.

	Heat day	No heat day
Block	a	b
No block	c	d

With the variables shown in the contingency table (Table 3), the following equation for the OR could be formulated:

$$OR = \frac{a/b}{c/d} \tag{2}$$

The fraction a/b describes the odds for a heat day when a block is present, and the fraction c/d describes the odds for a heat day when no block is present. Therefore, an OR greater than one means that the occurrence of a block increases the odds for a heat day. In contrast, an OR smaller than one means that the absence of a block increases the odds for a heat day. However, the OR does not give any information about the causality between blocks and heat days, only about the co-occurrence.

Here the information heat day/no heat day was taken from the heat regions, while the information block/no block was taken from each grid point in the European domain individually. Thus, the OR of a particular grid point tells whether a block at this grid point is conducive to heat in the considered region

or not. A block at a grid point was identified if the grid point was blocked at least once during a whole day. This way the 6-hourly temporal resolution of the blocking files was reduced to a daily resolution. The grid points where the JJA climatology of the individual blocking index is smaller than 0.5% were replaced with missing values in order to prevent high ORs due to a low climatology.

3.7.4 Blocks With/Without Heat

By cause of the odds ratio associated with the WE heat region, it was realized that SCH10 detects multiple blocks that occur while no heat day occurs (Section 4.4). Therefore, it was further investigated why during some SCH10 blocks WE heat days occur, and during other SCH10 blocks they do not.

For this, a block region was defined (5° W to 15° E, and 50° N to 60° N) based on the previously computed heat day composites (Figure 12). All blocks with their mean coordinates inside the block region at least once during JJA 1979 to 2015 were selected, in total 101 blocks.

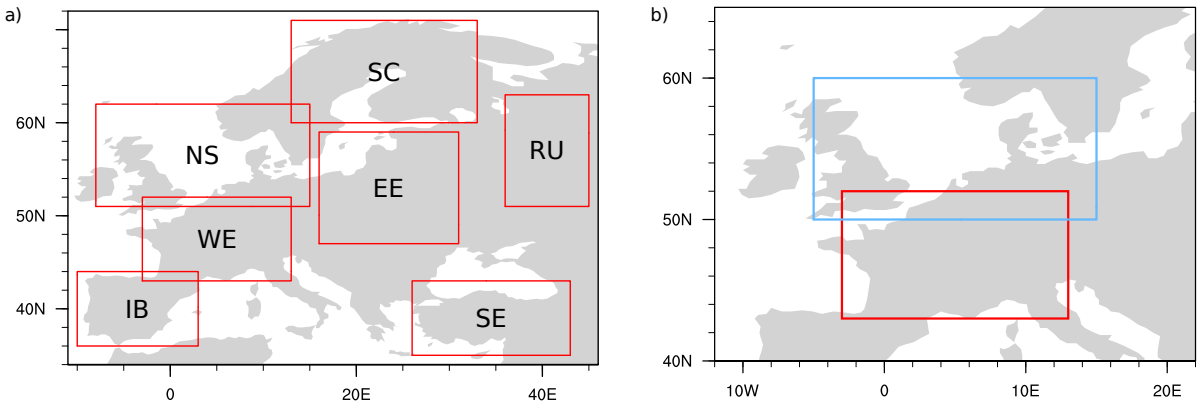

Figure 3: Maps of Europe with a) the seven heat regions (red boxes), and b) the western European heat region (red box) together with the corresponding block region (blue box).

All selected blocks that were inside the block region when a WE heat day occurred were assigned to the group of blocks with heat, in total 13 blocks. All other blocks were assigned to the group of blocks without heat (Figure A20). The blocks with heat spent 33 days in the block region, and the blocks without heat 136 days.

For both groups, the composites during the days in which the blocks were inside the block region were computed for the WSDI, the blocks, the GPH at 500 hPa, the daily maximum of T2m, and the volumetric soil water content into a soil depth of 0.28 m. On the one hand, these composites served to check whether the two groups could be separated from each other, and whether the blocks of the two groups were at the same location. On the other hand, the volumetric soil water content served to assess

the meteorological preconditions.

Additionally, the blocks of the two groups were compared by means of different attributes: the time inside the block region, the maximum area, and the minimum APV' value. Both groups included one block for which the area computation failed (Section 3.4); these blocks were ignored.

Finally, the number of heat grid points in the WE region were counted on the day when each block entered the block region, on the three preceding days, and on the three following days. This analysis aimed to test whether the time each block spends inside the block region is crucial for the development of heat or not.

4 | Results and Discussions

4.1 Block Characteristics

4.1.1 Results

Here the results from the comparison of the JJA blocks are presented. First the blocking frequencies of each index are treated individually, followed by the assessment of the blocks' characteristics. Concretely, it is shown *where on the northern hemisphere the blocking indices detect blocks during summer*, *what the differences between the indices' summer blocking frequencies are*, and *whether these differences can be explained in relation to the number, duration and size of the blocks*.

The blocking frequency of the TM2D index shows two latitudinal bands of high values. One of them lies north of $\sim$50°N, and one south of $\sim$50°N (Figure 4.a). The three maxima, exceeding 22%, are at low latitudes in the Pacific, North America and the Atlantic. At high latitudes, the maximum reaches 18% and is located between the Asian and American continent, near the Bering Strait. Two local maxima are located over Scandinavia and Greenland.

The index RO200 detects the maximum blocking frequency south of the Bering Strait (Figure 4.b). Compared to the other indices the frequency values are small, not exceeding 10%. This index's blocks are at mid- and high latitudes. Overall, this index's spatial distribution is similar to SCH13's.

The SCH indices detect three blocking frequency maxima that are located in the North Atlantic, the Arctic, and south of the Bering Strait (Figure 4.c-e). Hence, the spatial distribution is similar to the pattern of RO200. Depending on the chosen threshold, the maxima exceed 6% (-1.3 pvu), 18% (-1.0 pvu), or 22% (-0.7 pvu). Moreover, the higher the threshold is set, the further south the blocks are detected. Like TM2D, SCH07 reaches into subtropical latitudes.

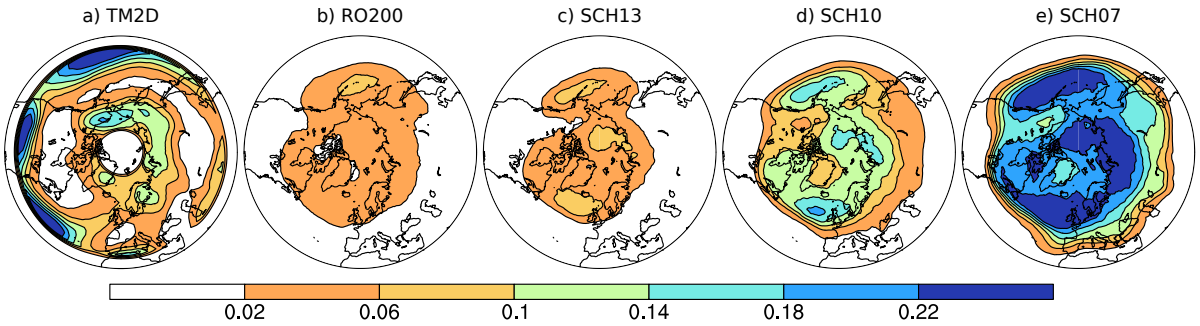

Figure 4: Northern hemispheric JJA blocking frequencies of the block detection indices a) TM2D, b) RO200, c) SCH13, d) SCH10, and e) SCH07 over the period from 1979 to 2015.

The two indices TM2D and SCH10 find the highest number of blocks per summer (Figure 5.a), while RO200 and SCH07 report the fewest blocks per summer. SCH13's number of blocks lies between the other two SCH indices. The total number of summer blocks over the period from 1979 to 2015 is 941 for TM2D, 325 for RO200, 679 for SCH13, 868 for SCH10, and 357 for SCH07.

The smallest blocks are captured by SCH13, and the largest by RO200 (Figure 5.b). TM2D reports smaller blocks than RO200, but still bigger blocks than the three SCH indices. Compared with TM2D and RO200, the three SCH indices have a larger range of block sizes. Above all, SCH07 covers various sizes exceeding the range of SCH10. Despite this, the median block size of SCH07 is smaller than that of SCH10, meaning that SCH07 includes more small blocks than SCH10.

All five blocking indices show median lifetimes between 8 and 10 days (Figure 5.c). SCH10 stands out with the highest median and the largest inter-quartile range. Equally, SCH07 stands out with some extremely long-living blocks. In fact, multiples of SCH07's blocks reach the maximum lifetime (177.5 days) defined by the code. Again, SCH07 has a lower median than SCH10.

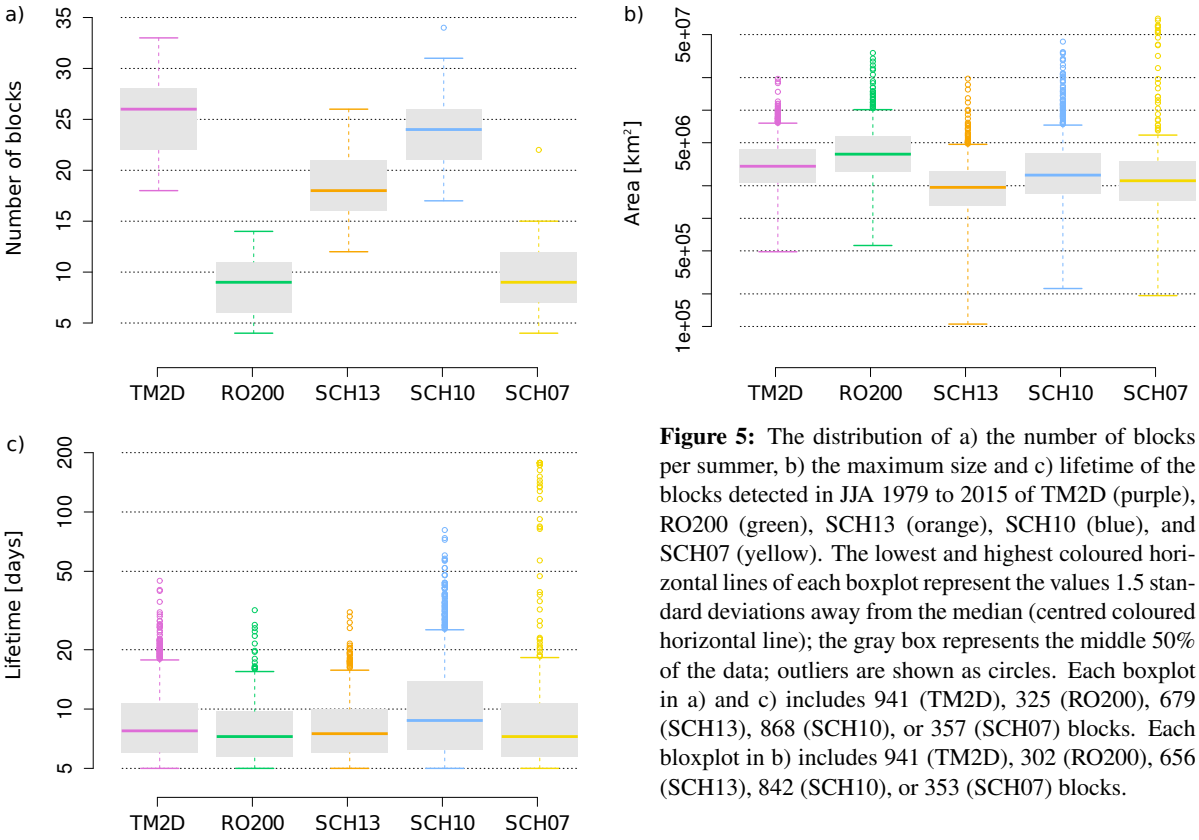

Figure 5: The distribution of a) the number of blocks per summer, b) the maximum size and c) lifetime of the blocks detected in JJA 1979 to 2015 of TM2D (purple), RO200 (green), SCH13 (orange), SCH10 (blue), and SCH07 (yellow). The lowest and highest coloured horizontal lines of each boxplot represent the values 1.5 standard deviations away from the median (centred coloured horizontal line); the gray box represents the middle 50% of the data; outliers are shown as circles. Each boxplot in a) and c) includes 941 (TM2D), 325 (RO200), 679 (SCH13), 868 (SCH10), or 357 (SCH07) blocks. Each bloxplot in b) includes 941 (TM2D), 302 (RO200), 656 (SCH13), 842 (SCH10), or 353 (SCH07) blocks.

4.1.2 Discussion

The comparison of the summer blocking frequencies reveals that TM2D detects the blocks at different locations than the other indices. These differences can be explained by the definition of a block as an anomaly in the case of RO200 and the SCH indices, in contrast to the blocking definition as a reversal of the meridional GPH gradient in the case of TM2D. Besides the location, differences were found in the values of the blocking frequencies. The causes of these differences lie in the number, size, and lifetime of the blocks.

The TM2D blocks in the subtropics are included in the number, size, and lifetime analysis. Thus, the high number of blocks detected by TM2D fits its high summer blocking frequency values observed in the subtropics. Similar reasoning can be applied to SCH10, which also finds many blocks and shows high frequencies. However, it seems contradictory that SCH07 - detecting by far the highest blocking frequency values - finds fewer blocks than TM2D or SCH10. To get these results, SCH07 must include large and/or long-living blocks.

Both are true: SCH07 detects the largest and the most persistent blocks. In other words, it is likely that SCH07 identifies one large block, while TM2D and SCH10 identify multiple blocks in the same area.

In the same way, SCH07 may find one long blocking period, while TM2D and SCH10 interpret the same time window as multiple blocking periods.

The observation that SCH13 finds more blocks than RO200 is surprising because the two indices have very similar blocking frequencies. Again, the explanation could either lie in the size or in the lifetime of the blocks. The two indices' blocks have very similar lifetime distributions. Again, the size distribution is such that SCH13 may identify multiple blocks in the same area in which RO200 detects only one block.

As stated in the results (section 4.1.1), the lower median of SCH07 compared to SCH10 suggests that SCH07 includes many small blocks. It is assumed that these blocks are weak anomalies that are not detected by SCH10 or SCH13. Possibly these blocks are also short-lived and contribute to the relatively low median lifetime of SCH07's blocks.

4.2 Threshold Choice

4.2.1 Results

In this section the topic of the different intensity thresholds for the SCHWIERZ et al. (2004) index is addressed. By looking at the distribution of the APV', it is shown *what percentile -1.3, -1.0, and -0.7 pvu represent in the extratropical summer distribution of the APV'*, and *what fraction of the APV' values per latitude that fall below a threshold is classified as blocks*.

The computation of the extratropical summer APV' distribution revealed that -1.3 pvu corresponds to the lowest 2.74% , -1.0 pvu to the lowest 6.46%, and -0.7 pvu to the lowest 14.08% of the values. If each latitude is considered individually, the percentage of the APV' values per latitudes that are smaller than a certain threshold increase with increasing latitude. North of $\sim$50°N the APV' values below the three thresholds correspond approximatively to the lowest 6% (-1.3 pvu), 12% (-1.0 pvu), or 22% (-0.7 pvu) of each latitude's APV' distribution (Figure 6.a).

The comparison to the zonal mean of the corresponding blocking index reveals that most of the APV' values below a certain threshold are classified as blocks. On average, across all extratropical latitudes, 62% (-1.3 pvu), 77% (-1.0 pvu), and 90% (-0.7 pvu) of the APV' values that are smaller than the demanded threshold also fulfil the persistence and stationarity criteria. These percentages are not only dependent on the threshold, but also on the latitude (Figure 6.b).

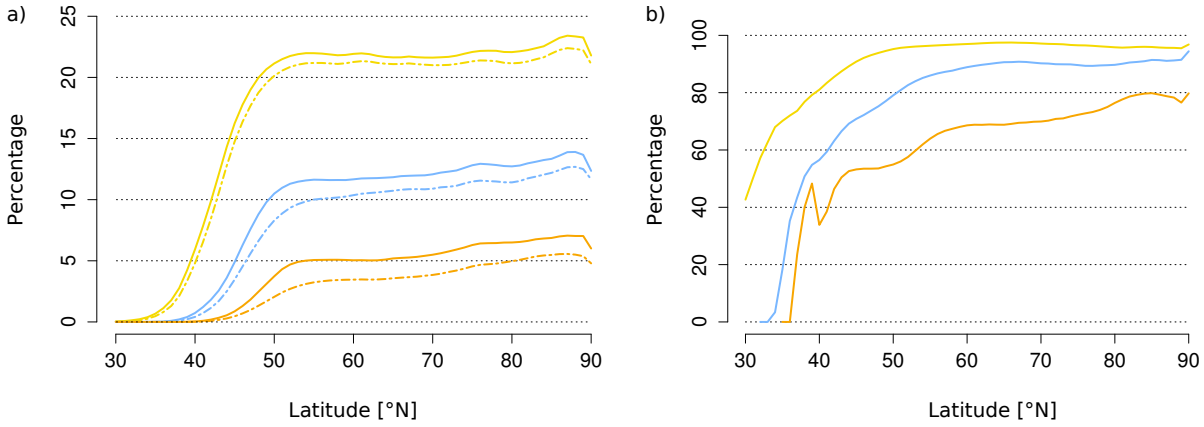

Figure 6: Left: The percentages of the APV' values (from JJA 1979 to 2015) per latitude that are smaller than the threshold -1.3 (orange line), -1.0 (blue line), and -0.7 pvu (yellow line), and the zonal mean of the blocking frequencies (from JJA 1979 to 2015) of the index SCH13 (orange dashed line), SCH10 (blue dashed line), SCH07 (yellow dashed line). The zonal mean of the blocking frequency (from JJA 1979 to 2015) divided by the percentage of the APV' values (from JJA 1979-2015) per latitude smaller than the corresponding threshold -1.3 (orange line), -1.0 (blue line), and -0.7 pvu (yellow line).

4.2.2 Discussion

It has been shown that the choice of the thresholds for the SCH index is crucial. The three values -1.3, -1.0, and -0.7 pvu represent very different percentiles. SCHWIERZ et al. (2004) determined -1.2 pvu as a threshold with the reasoning that this value corresponds to the lower 10% of the extratropical year-round APV' distribution. With the percentages found here, i.e. 2.74% (-1.3 pvu) and 6.46% (-1.0 pvu), -1.2 pvu is assigned to a smaller percentile than proposed by SCHWIERZ et al. (2004).

There are multiple reasons for this inconsistency: SCHWIERZ et al. 2004 used different data (ERA15); defined the anomaly relatively to a 15-year monthly mean instead of the 30-day running mean as used here; and may have set the border between tropics and extratropics at a different latitude. Furthermore, only JJA are considered here, while SCHWIERZ et al. (2004) included the APV' values of all four seasons in the APV' distribution. However, the APV' distribution is heavily dependent on the season (Section A.4).

The percentage of APV' values smaller than -1.3 pvu reveals that the blocking index SCH13 is not able to detect a block south of 40°N. In other words, the choice of the intensity threshold directly determines at which latitudes blocks can be detected. This gives a reason to consider the use of the SCHWIERZ et al. (2004) index with seasonal or latitudinal-dependent thresholds. If an index with alternating intensity thresholds were created, one would need to consider the seasonal variations of the storm tracks. Both, the Pacific and Atlantic, storm tracks migrate equatorward in fall, and poleward in spring. The Pacific storm track is strongest in spring and fall, while the Atlantic storm track reaches its maximum intensity in midwinter (CHANG et al. 2002). With regard to the detection of European summer blocks, the fact

that the Atlantic storm track is especially north in summer supports a low (e.g. -1.3 pvu) block intensity threshold; however, the fact that the Atlantic storm track is especially weak in summer supports a high (e.g. -0.7 pvu) block intensity threshold.

4.3 Case Studies

4.3.1 Results

In the first part of this section, the case studies are summarized and the results for each blocking index are presented. In the second part, the four cases of 1994, 2010, 2003 and 2007 are given as examples. More precisely it is assessed *which of the blocking indices detect a block during the selected European heat events*, and *where the blocking indices are positioned relative to each other and relative to the heat index during the selected European heat events*.

The three cases 1994, 2010, and 2003 are chosen because each of them represents one of the three blocking patterns introduced in the literature review (Chapter 2): the dipole block, the omega block, and the stationary, high-amplitude ridge. The case 2007 is chosen because it shows the fourth stationary flow pattern: the stationary, low-amplitude ridge. Additionally, RUSSO et al. (2015) assigned the four events to the top ten European heat waves since 1950. For the remaining cases, similar information is given in the Appendix (Section A.5).

4.3.1.1 Summary Case Studies

All seven heat waves are captured by the two heat indices: The WSDI appears in the areas and time windows proposed by the literature. In the same manner, the HUMIDEX displays the heat waves as areas with values from 30 to 39, i.e. “some discomfort”. The WSDI shows the largest area in 2003. Contrastingly, the HUMIDEX finds the largest area of such high values in 2010. In all cases at least two of the blocking indices respond (Table A3).

The blocking index TM2D finds a block in all cases except for 2003, where no reversal of the meridional gradient occurred. In 2010 and 2006 - both omega blocks - TM2D detects two blocks. These two blocks are located south-west and south-east of the ones reported by the other indices. In all other cases TM2D finds one block centred slightly south of the anomaly-based indices. TM2D occupies a smaller area compared to SCH10, SCH07 and RO200. In 1994 and 2007 the TM2D block is co-located with the WSDI, while in all other cases the block and heat overlap only marginally.

Table 4: Case studies listed according to the year and region together with the responding block detection indices and the flow type (1 = dipole block; 2 = omega block; 3 = stationary, high-amplitude ridge; 4 = stationary, low-amplitude ridge).

Year	Region	TM2D	RO200	SCH13	SCH10	SCH07	Type
1994	Scandinavia	✓		✓	✓	✓	1
2003	Central Europe		✓	✓	✓	✓	3
2006	Central Europe	✓			✓	✓	2
2007	Greece	✓				✓	4
2010	Russia	✓	✓	✓	✓	✓	2
2013	British Isles	✓			✓	✓	1
2015	Central Europe	✓	✓		✓	✓	1,3

The blocking index RO200 finds a block in 2003, 2010, and 2015. These three events show a large coherent WSD area coinciding with HUMIDEX values of 30 to 39. Nevertheless, the events in 1994 and 2007 - both cases with large heat areas - remain undetected. If RO200 and the SCH indices both detect a block, they usually agree on the location. The size of the RO200 blocks are comparable to the SCH07 blocks. RO200 and SCH07 overlap the most with the WSDI.

The blocking index SCH13 appears in 1994, 2003, and 2010, while SCH10 detects a block in all cases except for the stationary, low-amplitude ridge in 2007. Finally, SCH07 finds a block in all seven cases. The SCH indices are centred at the same location, but the size of the block grows with an increasing APV' threshold. Compared to the remaining indices, SCH13 finds the smallest blocks and SCH07 the largest. The WSDI is either co-located or south of the SCH indices.

4.3.1.2 Dipole Block 1994

A heat wave took place in southern Scandinavia and central Europe (FISCHER et al. 2007, RUSSO et al. 2015) in July and August 1994. The heat was most severe in eastern Germany and Poland (RUSSO et al. 2015). According to FISCHER et al. (2007), the extreme temperatures were caused by anomalous southerlies that transported warm and dry air from the Mediterranean region northwards.

In the analysis, the SCH indices detect a block from July 25th onwards, while TM2D appears first on July 27th (Figure 7.a). The four indices agree on the block's location over the Baltic States (Figure 7.c). On July 30th the block starts to weaken and then disappears. During the whole blocking episode, high APV air is south of the low APV of the block (Figure 7.a,7.c); thus, the block is a reversal block.

According to the WSDI, eastern Germany, Poland, and the Baltic States experience WSDs from July 21st to August 3th. The HUMIDEX shows "some discomfort" in the same region, but from July 27th

to August 2nd. Both heat indices' spatial extension is largest from July 27th (Figure 7.c) to July 29th (Figure 7.d). During the whole blocking episode, the heat indices are partly co-located with, and partly south of, the two blocking indices (e.g. Figure 7.b,7.d).

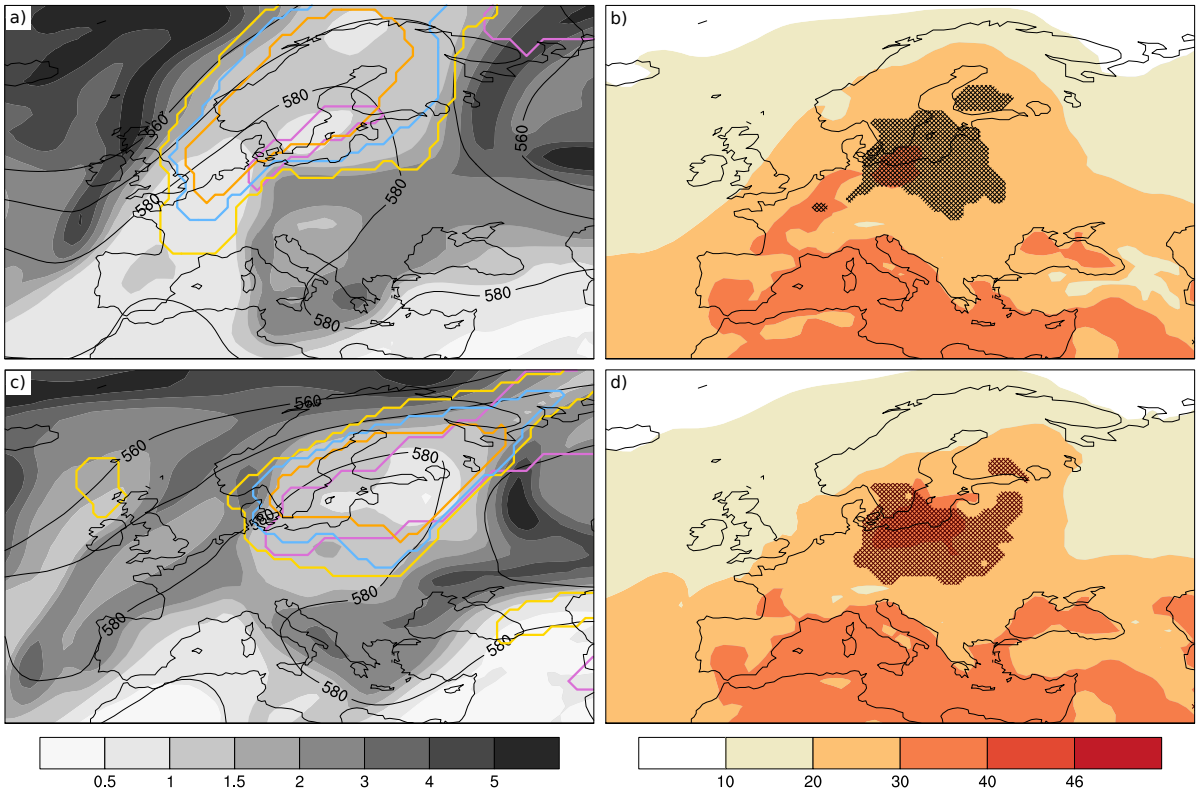

Figure 7: Left: Vertically-averaged (500 to 150 hPa) PV [pvu] (shading), GPH [gpdm] on 500 hPa (black contours), blocking index TM2D (purple), RO200 (green), SCH13 (orange), SCH10 (blue) and SCH07 (yellow). Right: HUMIDEX (shading), WSDI (black hatching). Shown is a)-b) July 27th 1994 at 12 UTC, and c)-d) July 29th 1994 at 12 UTC.

4.3.1.3 Omega Block 2010

From the middle of June to the middle of August 2010 a block lead to heat and drought conditions in Russia, Belarus, Ukraine and the Baltic. The block over western Russia also caused anomalous high precipitation and floods in Pakistan (SCHNEIDEREIT et al. 2012, LAU and KIM 2012).

In the analysis, multiple blocking episodes are observed from the middle of June to the middle of August. The first block - detected by SCH07, SCH10, and TM2D - develops over the British Isles on June 24th, moves across the North Sea and the Baltic States, and reaches western Russia on July 2nd. The second block - detected by SCH07, SCH10, TM2D, and RO200 - again develops over the British Isles on July 1st and moves over Scandinavia to western Russia were it weakens on July 9th. The third block - detected by all five indices - develops over the North Atlantic on July 6th, strengthens over the North Sea, and reaches western Russia on July 13th. While the third block remains over western Russia, a fourth block - also detected by all five indices - develops over the North Sea on July 19th,

moves towards western Russia and replaces the third block on July 21st. This fourth block remains over western Russia until it decays on August 1st. Only two days later, on August 3th, a fifth block develops over western Russia - again detected by all five indices - and remains there until it weakens and disappears on August 13th.

During all five blocking episodes the WSDI appears, and the HUMIDEX reports "some discomfort" near the block. The areas affected by heat are the largest during the last two of the five episodes. The omega pattern is best visible during the fourth episode. Therefore, this blocking episode is described below in more detail:

The indices SCH07 and SCH10 find a block over the North Sea on July 19th. The block moves to western Russia and is detected by SCH13 and TM2D on July 21st, and by RO200 on July 25th. At the beginning, all SCH indices are centred north of TM2D, and the block resembles a dipole block (Figure 8.a). Later, the pattern changes to an omega block. At this stage RO200 and SCH07 cover a large T-shaped area, while SCH10 describes one zonally elongated block north of two TM2D blocks (Figure 8.c). The index SCH13 vanishes on July 26th, the other indices on August 1st.

When the heat area is the largest, on July 29th (Figure 8.d), the HUMIDEX indicates "some discomfort" over an area reaching from Finland to the Caspian Sea. At the same time, the WSDI shows a smaller area in the centre of the indices RO200 and SCH07. During the whole blocking episode RO200 and SCH07 overlap the most with the heat indices, while SCH10 is to the north, and TM2D is shifted to the west and east.

4.3.1.4 Stationary, High-Amplitude Ridge 2003

In summer 2003 two heat waves occurred in Europe, the first one in June and the second one during the first two weeks of August. Both episodes were related to a ridge over western Europe that was absent during July (GARCÍA-HERRERA et al. 2010, Figure 2). The temperature anomalies were stronger in the latter episode (GARCÍA-HERRERA et al. 2010), therefore this episode is analysed below. Z'GRAGGEN (2006) found that the advection of warm air, the subsiding motion east of the ridge's axis, and the dry soil conditions led to the heat wave in August.

SCH07 and SCH10 detect a block that develops over the North Pacific on July 31st. The block moves east and becomes stationary over western Europe. On August 5th the block grows northwards and strengthens such that SCH13 appears. Until August 11th a high-amplitude ridge is found over central and northern Europe: low APV air stretches from low to high amplitudes bounded by high APV air up-

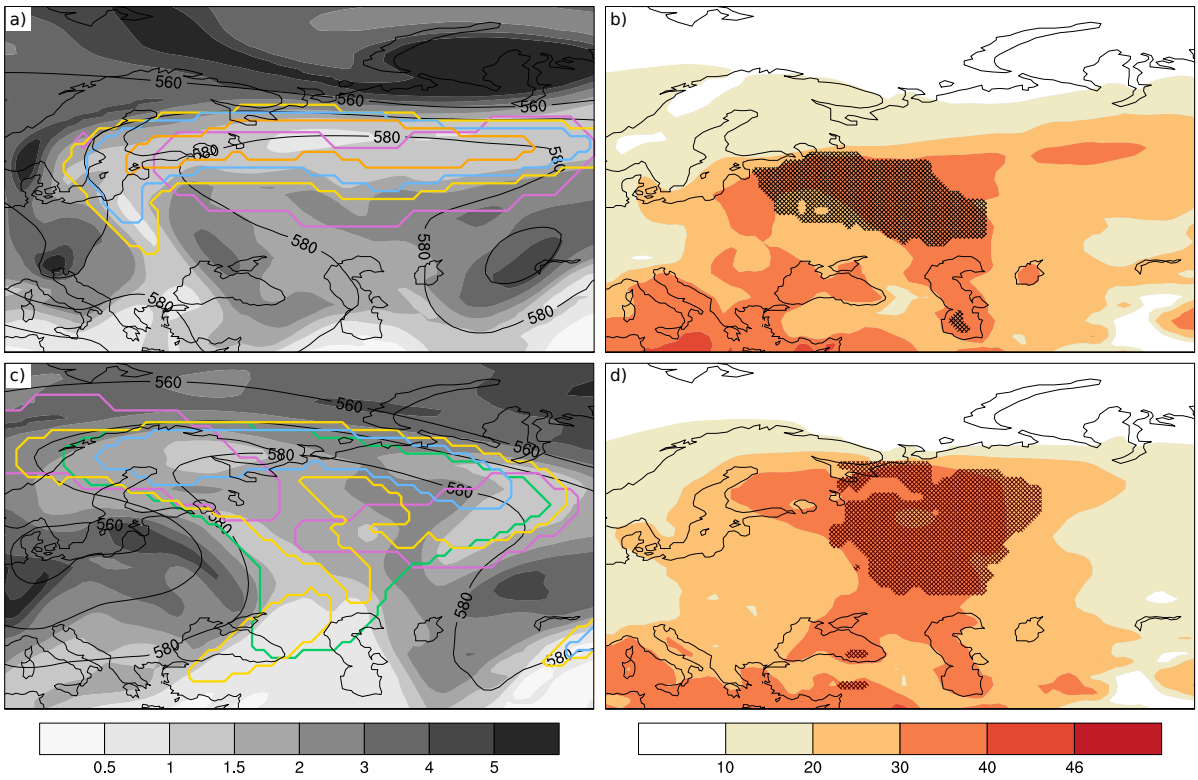

Figure 8: Same as Figure 7 but for a)-b) July 24th 2010 at 12 UTC, and c)-d) July 29th 2010 at 12 UTC.

and downstream. The SCH indices and RO200 agree on the location of the ridge (Figure 9.a, 9.c). On August 12th only SCH07 and SCH10 are left, and on August 16th all blocking signals are gone.

The WSDI starts to detect a WSD on August 2nd, first in southern Europe and then also further north. The largest extension of the WSDI is reached on August 9th (Figure 9.d) when a WSD is found in the whole of western Europe, the British Isles, and on the North Atlantic Ocean near Iceland. On August 12th the WSD disappears from western Europe, but remains over the Mediterranean Sea until the end of August. During the whole blocking episode the heat indices in central Europe are mostly south of the blocking indices (e.g. Figure 9.b), while the WSD area near Iceland lies mostly west of the blocking indices (e.g. Figure 9.d).

4.3.1.5 Stationary, Low-Amplitude Ridge 2007

A heat wave affected Greece, Italy, the Balkans, and Cyprus in June 2007. In Greece the heat wave lasted from June 24th to 28th. On June 26th 44.8° C were measured in Athens, representing the highest measured temperature since 1897. The extreme temperatures developed due to an anticyclone above the central Mediterranean which transported Saharan air masses and caused large scale subsidence (KOTRONI et al. 2011).

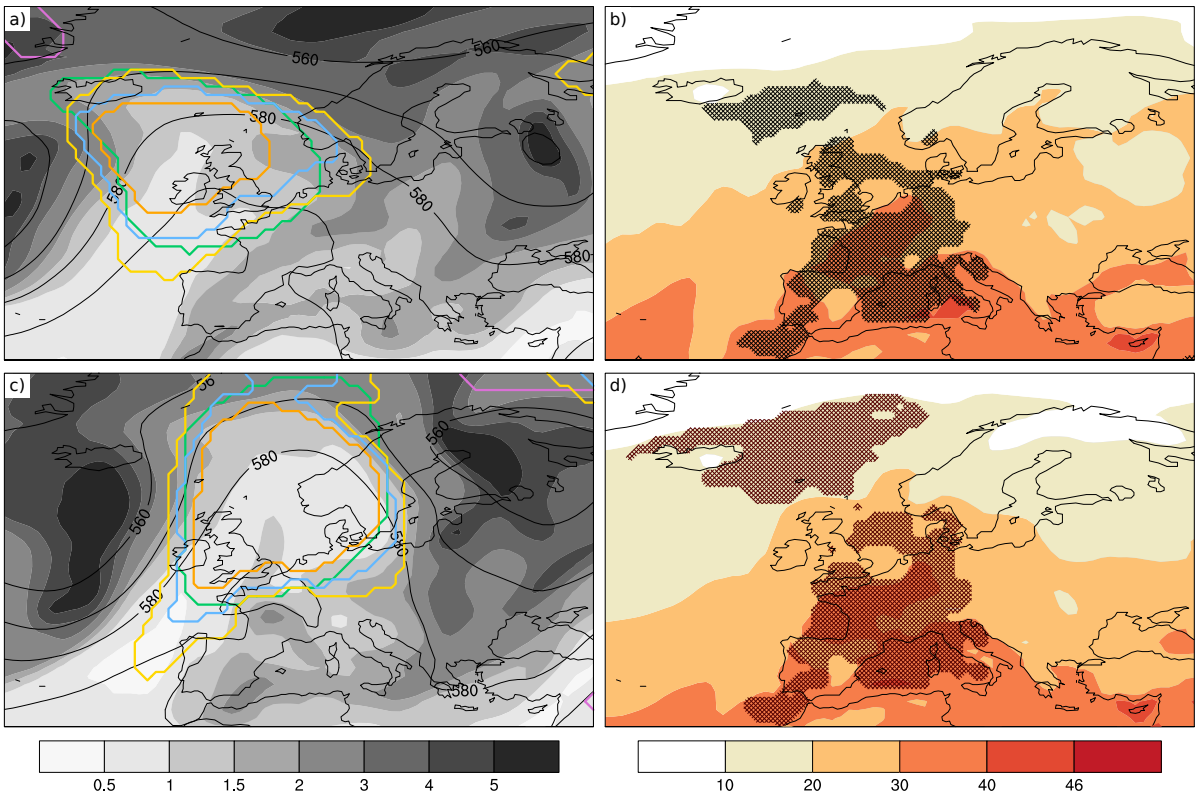

Figure 9: Same as Figure 7 but for a)-b) August 8th 2003 at 12 UTC, and c)-d) August 9th 2003 at 12 UTC.

The index TM2D finds a block over the Mediterranean Sea south of Italy on June 18th. SCH07 detects a block over Italy on June 19th. From June 21st to 26th (Figure 10) the two blocking indices embrace Italy, the Balkans, and Greece (Figure 10.a,10.c). TM2D weakens and disappears on June 26th (Figure 10.c), while SCH07 remains for one more day. The low APV air from the ridge does not reach into high latitudes, therefore the atmospheric feature recognized by SCH07 and TM2D is a stationary, low-amplitude ridge.

The WSDI first finds a WSD on June 19th in Greece and the Adriatic Sea. From then on the WSD area grows towards the Balkans, reaches its largest extension on June 25th (Figure 10.b), and disappears on June 28th. In the same regions the HUMIDEX indicates “some discomfort”, and from June 24th to 28th some regions experience “great discomfort” (Figure 10.b,10.d). From June 30th on HUMIDEX values greater than 30 are only found over the Mediterranean Sea and no longer over land masses. During the whole blocking episode the two blocking indices are co-located with the two heat indices.

4.3.2 Discussion

A selection of heat wave cases have been shown in which observations regarding the presence, the size, and the location of the various blocking indices were made. These observations can be explained with

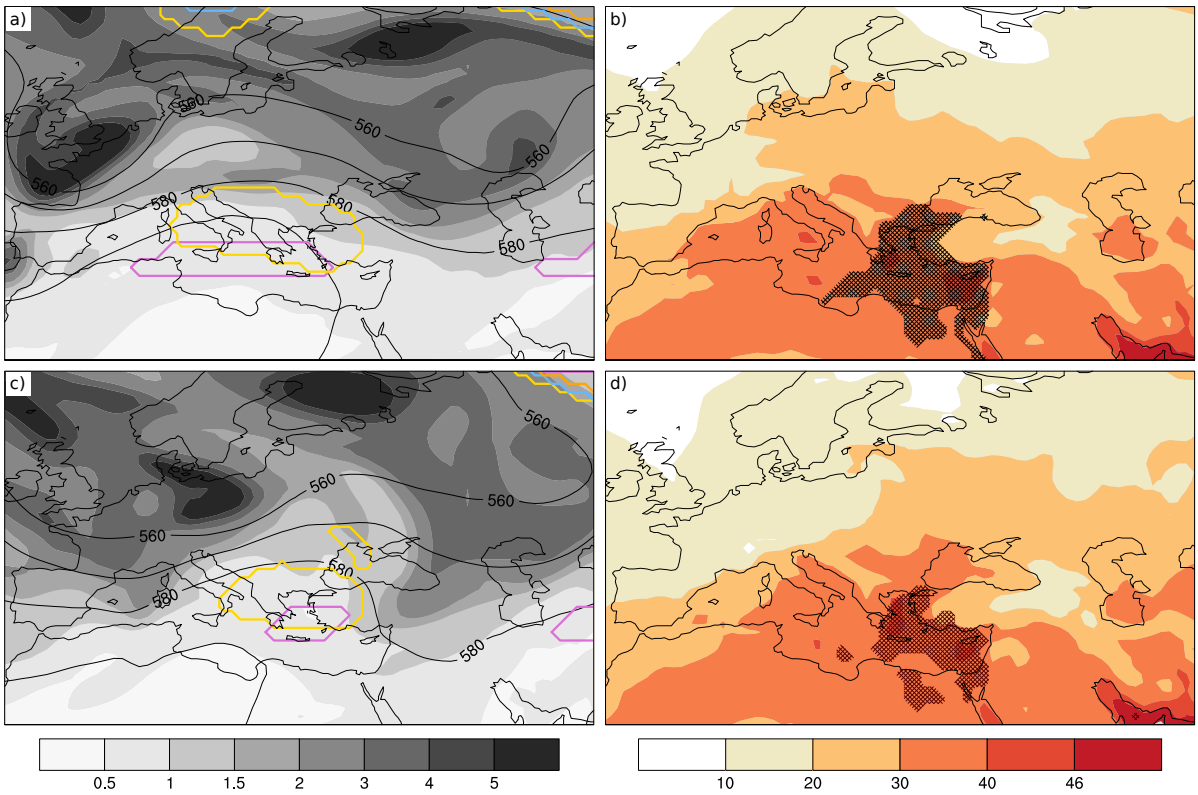

Figure 10: Same as Figure 7 but for a)-b) June 25th 2007 at 12 UTC, and c)-d) June 26th 2007 at 12 UTC.

the different definitions of the blocking indices. Due to its definition as a reversal of the GPH gradient, TM2D is expected to detect the blocks south of the blocks found by the anomaly-based indices. In addition, TM2D should detect two blocked regions in the case of an omega block (e.g. cases 2006, 2010), and should not be able to identify a block in the case of an untilted stationary ridge (e.g. case 2003).

Moreover, it makes sense that RO200 is sensible to events with large areas of heat, because RO200's blocks are directly related to high temperatures through their definition as a positive GPH anomaly. The link between GPH anomalies and absolute temperature values can be found in the thickness equation (Equation A3). ROHRER (2017b) pointed out that the use of RO200 may be problematic due to its temperature dependency by showing that the blocking frequency of RO200 and the temperature anomaly in the same domain are positively correlated (Figure A4).

The GPH field displays a smoothed version of the PV field (HOSKINS 1985). Thus, the SCH indices and the RO200 index are expected to identify blocks that appear at the same location, as observed. Additionally, the finer structure of a PV field compared to a GPH field, explains the more detailed structure of the SCH indices compared to RO200 (e.g. case 2010).

In accordance with the indices' summer blocking frequencies (Figure 4), TM2D and SCH07 found blocks at low latitudes, since they interpreted subtropical high pressure systems as blocks (e.g. case 2007). Finally, it could be demonstrated that SCH07 indeed covers a variety from small to large blocks (e.g. case 2010), as it was hypothesized in Section 4.1.

For the following investigation of the block-heat relation, the case studies have shown that it is certainly important which blocking index is used. For instance, if exclusively the index SCH13 is used exclusively, few of the heat events will be related to blocks, while SCH07 proposes a relation in all cases. In my opinion, the index SCH13 defines blocks too narrowly, because it misses important events like in 2006, 2013, and 2015. Equally, the index SCH07 defines blocks too broadly, because it recognizes the subtropical high of 2007 as a block. Therefore, I decided to use SCH10 and to ignore SCH13 and SCH07 in the subsequent analysis. The argument against SCH07 could be used for TM2D as well. However, I wanted to keep TM2D as the only reversal index in the analysis.

From the case studies it is further expected that RO200 will show the highest co-occurrence in time and space with the heat waves (e.g. cases 2003, 2010). Additionally, TM2D is expected to have a spatial block-heat distribution noticeably different from the ones of SCH10 and RO200.

The WSDI was observed to be extended south of the blocking indices. Therefore, it is preferable to include remote effects in the analysis of the spatial block-heat relation. On the scale of grid points, one might miss the relation between heat and block regions that are not co-located.

4.4 Blocks and Heat

4.4.1 Results

In the case studies it was shown how the blocking indices perform during single events. Here the relation between blocks and heat is analysed from a climatological perspective. First the blocking indices TM2D, RO200, and SCH10 are compared during the heat days of the Scandinavian (SC) and the western European (WE) region. It is shown *how often (relative to the summer climatology) each grid point is blocked when a European heat day occurs*, and *how the odds for a European heat day are changed when a block occurs*. Then, *the difference between the blocking episodes of the SCH10 that are associated with WE heat days and those that are not* is addressed by comparing the two groups of SCH10 blocks.

The SC and WE regions are chosen because they illustrate two distinct situations. The results for the

other heat regions are shown in the Appendix (Figures A11-A19).

4.4.1.1 Scandinavian Heat Region

During SC heat days (Figure 11), all three blocking indices find blocks in the SC region. The maximum blocking frequencies shown by individual grid points are 40% for TM2D, 20% for RO200, and 50% for SCH10. These values are considerably higher than the JJA (1979 to 2015) blocking climatologies: TM2D exceeds the climatology by 30%; RO200 by 10-20%; and SCH10 by 30% (Figure 11.d-f). With this, about 75% (TM2D), 50-100% (RO200), and 60% (SCH10) of the blocking-frequencies maxima shown in the composites (Figure 11.a-c) are deviations from the JJA climatology. TM2D associates negative blocking-frequency anomalies of -10% at the Algerian coast with SC heat days. SCH10 shows negative blocking-frequency anomalies of -10% west of Ireland. The anomalous GPH field shows an anticyclone centred above Scandinavia. The heat region lies in the centre of this anticyclone.

For all three blocking indices, the pattern of the ORs consists of values greater than one in northern Europe, and values smaller than one in southern Europe (Figure 11.g-i). In other words, the blocking indices agree that northern blocks are conducive to SC heat days, while southern blocks are unfavourable for SC heat days. In the SC region the blocking indices increase the odds for a heat day by a factor of 10.

4.4.1.2 Western European Heat Region

During WE heat days (Figure 12), TM2D detects blocks downstream of the WE region, while RO200 and SCH10 find blocks north of the WE region. The maximum blocking frequencies shown by individual grid points are 10% for TM2D, 20% for RO200, and 40% for SCH10. Again, these values are considerably higher than the JJA (1979 to 2015) blocking climatologies: TM2D exceeds the climatology by 10%; RO200 by 10-20%; and SCH10 by 20-30% (Figure 12.d-f). With this, about 100% (TM2D), 50-100% (RO200), and 50-75% (SCH10) of the blocking-frequencies maxima shown in the composites (Figure 12.a-c) are deviations from the JJA climatology. Only TM2D shows negative blocking-frequency anomalies of -10% at the Algerian Coast. The GPH shows that WE heat days are associated with a ridge. The heat region lies especially in the southern part of the ridge, and somewhat upstream of the ridge's axis.

The ORs are greater than one in the WE heat region for all three blocking indices. The maximum values are 5 (SCH10), 10 (TM2D), and 20 (RO200). For RO200, the area with ORs greater than 10 is expanded over the whole of western and central Europe, while for TM2D and SCH10, the high values

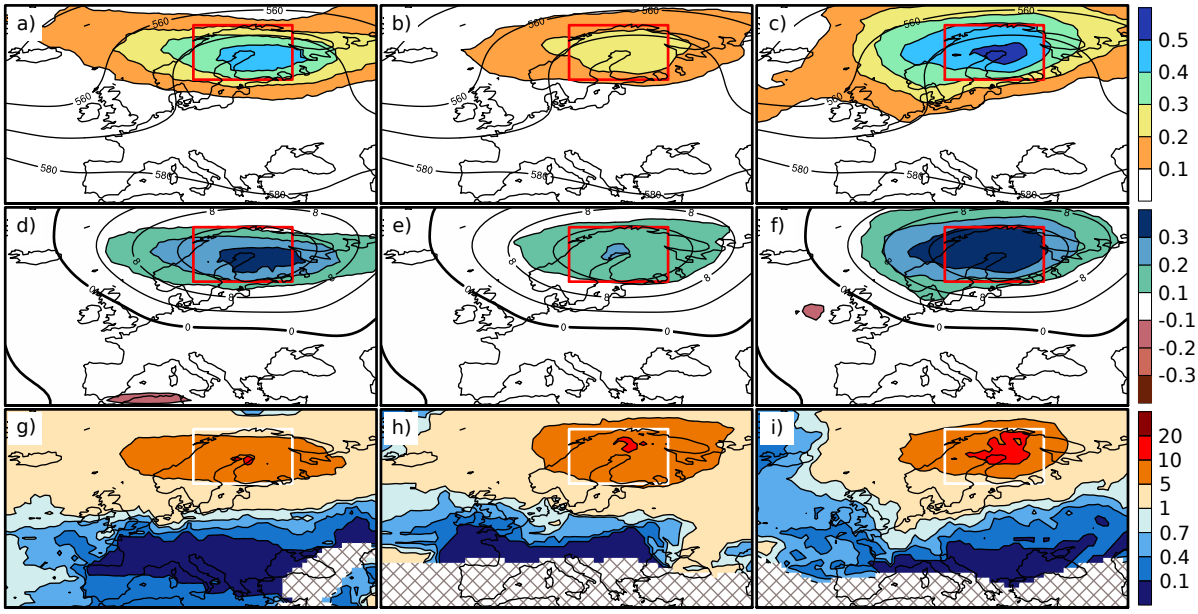

Figure 11: Top: Composites during heat days in the SC region (13° W to 33° E, 60° N to 71° N) of the blocking fields (shading) and of the GPH at 500 hPa (black contours) are shown in a) TM2D, b) RO200, and c) SCH10. Middle: The blocking frequency anomaly a), b), c) relative to the JJA blocking climatology (1979 to 2015) are shown in d) TM2D, e) RO200, and f) SCH10. The black contours in d), e), f) are GPH anomalies at 500 hPa relative to the JJA climatology in 4 hPa intervals; the thick line denotes 0 hPa, dashed lines negative anomalies, and thin lines positive anomalies. Bottom: The odds ratio between SC heat days with blocks and SC heat days without blocks is shown in g) TM2D, h) RO200, and i) SCH10. The red/white framed box represents the heat region. The regions where the JJA blocking climatology (1979 to 2015) of the individual blocking index is smaller than 0.005 are masked out. The maps show the European domain (25° W to 50° E, and 35° N to 75° N).

are located closer to the heat region. The Mediterranean and the Norwegian Seas are the regions in which the presence of a TM2D block decreases the odds for WE heat days. For RO200 and SCH10, blocks up- and downstream of the WE heat region decrease the odds for WE heat days.

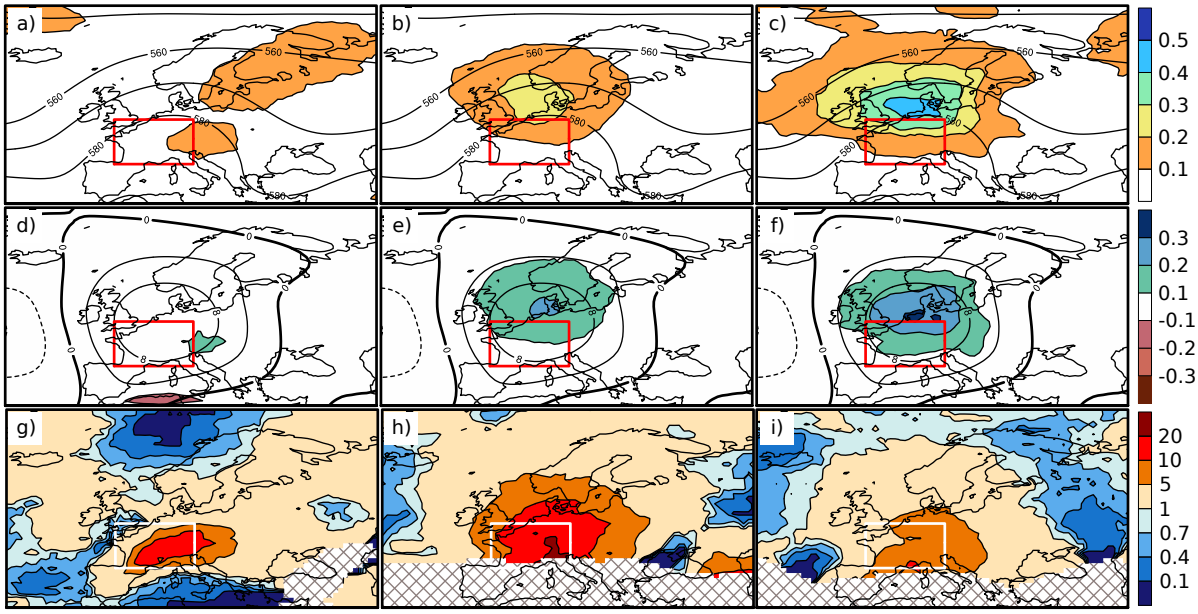

Figure 12: Same as Figure 11 but for the western European heat region (3° W to 13° E, 43° N to 52° N).

4.4.1.3 Blocks With/Without Heat

For SCH10, the blocks with heat and without heat in the WE region are compared. The composites of the WSDI show that the heat-day definition successfully separates the two groups of blocks. The WE grid points report a WSD during 20% of the 33 block days with heat (Figure 13.a); by contrast, a WSD is found in less than 2% of the 136 days without heat (Figure 13.b).

The composites of the blocks and the GPH show that the blocks of both groups are at the same location, but that the synoptic ridge is more pronounced for the blocks with heat than for the blocks without heat (Figure 13.c-d). The volumetric soil water content in the WE region is smaller during the blocks with heat than during the blocks without heat (Figure A.13.e-f). During the blocks with heat, the daily maximum temperatures reach 28°C in the WE region and 30°C southwest of it, on the Iberian Peninsula (Figure 13.g). The blocks without heat are related to lower daily maximum temperatures in the WE region, reaching only 26°C. However, on the Iberian Peninsula temperatures also reach 30°C (Figure 13.g-h).

The comparison of the blocks' attributes reveals that the blocks with heat stay longer in the block region than the blocks without heat. While the former are in the block region for 2.75 days (2.52 days) in the median (mean), the latter are in the block region for 1.25 days (1.55 days) in the median (mean) (Figure 14.a). No large differences are found in the intensity or the size of the blocks (Figure A21) during their time inside the block region.

The number of the WSD grid points in the WE heat region increases during the three days before the blocks with heat enter the block region. The heat-day threshold of 16 grid points is crossed on the day the blocks enter the region. One day later the maximum is reached, and the number of grid points decreases again. No such increase can be found when blocks without heat enter the block region (Figure 14.b).

4.4.2 Discussion

In the composites for the SC region (Figure 11) the blocks occur co-located with the heat, independent of the blocking index. However, TM2D and SCH10 are more frequent during SC heat days than RO200. This can be explained by the northern position of the SC region. RO200 is directly linked to absolute temperature values through the equation of thickness (Equation A3, Figure A4), and is therefore less sensible to heat in high latitudes where absolute temperature values are low. In short, with regard to the

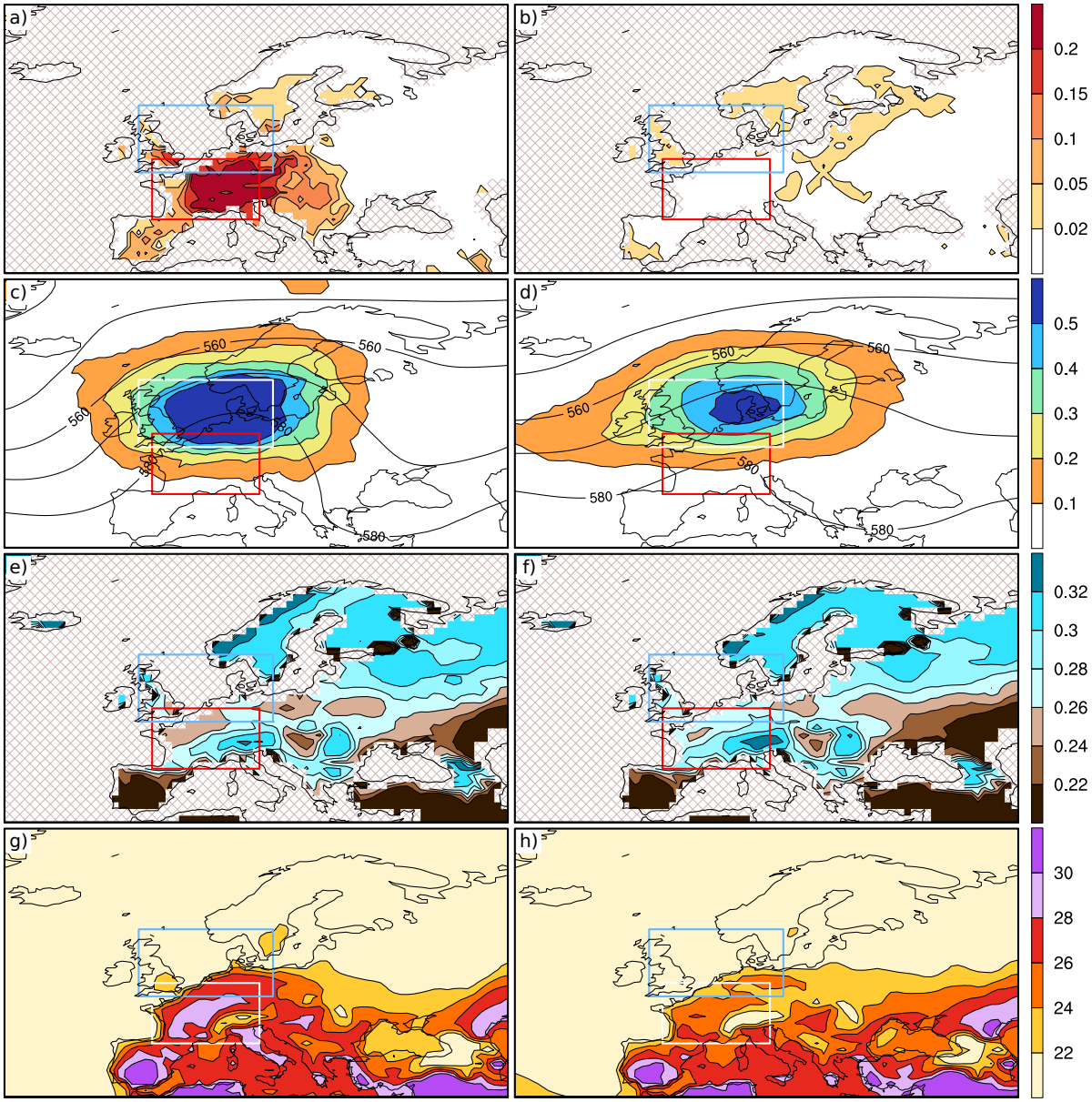

Figure 13: Left: Composites over the 13 blocks (33 days) with WE heat days. Right: Composites over the 88 blocks (136 days) without WE heat days. Shown are the composites of a)-b) WSDI; c)-d) SCH10 blocks (shading); c)-d) GPH (black contours); e)-f) volumetric soil water content [m^3m^{-3}]; and g)-h) daily maximum temperature two meter above ground [° C]. The red/white box represents the WE heat region, the blue/white box represents the block region. The maps show the European domain (25° W to 50° E, and 35° N to 75° N). Hatching indicates missing values.

location of the blocks, the choice of the blocking index does matters less than the absolute or anomalous blocking frequencies.

The ORs are greater than one and have a maximum of 10 in the SC region for all three blocking indices. So, independent of the index, the conclusion can be drawn that blocks in the SC region increase the odds for heat by a factor of 10. If there is a block in southern Europe that does not reach into high latitudes, then Scandinavia lies in the undisturbed climatological westerlies; thus the circulation gives no reason for heat in Scandinavia. This explains the ORs below one in southern Europe.

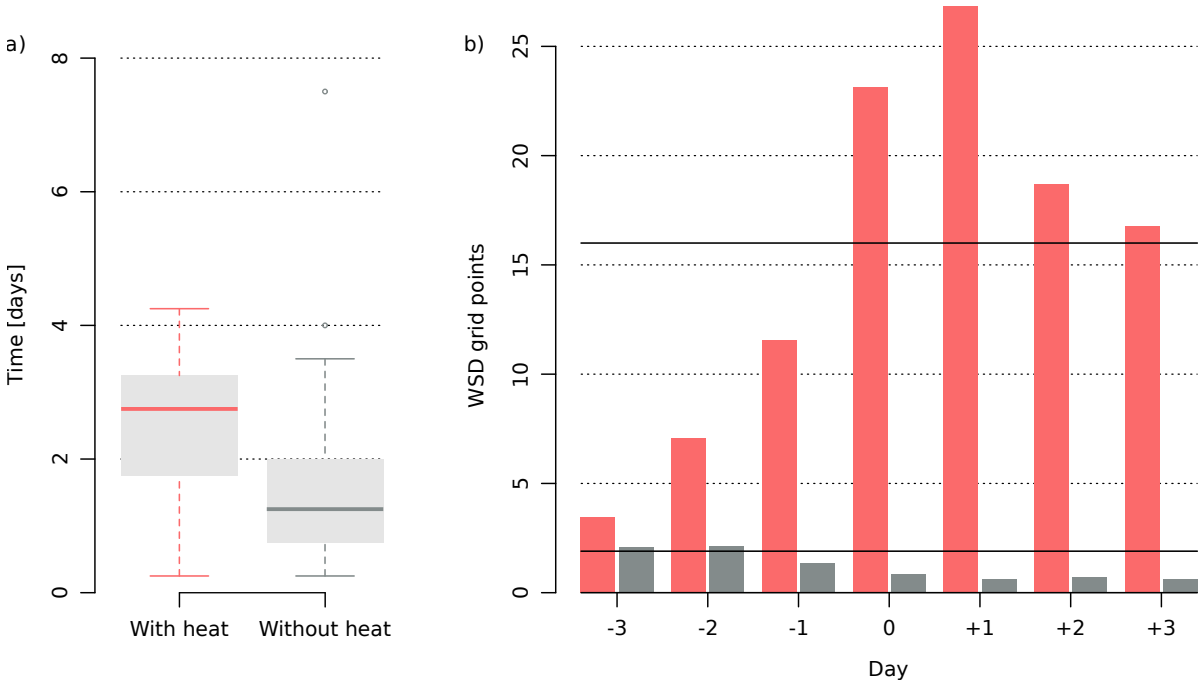

Figure 14: The boxplots in a) show the distribution of the days each block is in the block region (5° W to 15° E, and 50° N to 60° N). In the boxplots the lowest (highest) coloured horizontal line represents the lowest (highest) value not more than 1.5 standard deviations away from the median; the gray box represents the middle 50% of the data; the centred coloured horizontal line represents the median; values more than 1.5 standard deviations away from the mean are outliers and are shown as circles. The bars in b) show the mean number of WSD grid points in the WE region relative to the day when the blocks enter the block region (day 0). The lower horizontal black line shows the mean number of WSD grid points in the WE region during JJA 1979 to 2015. The upper horizontal black line shows the heat day threshold of 16 WSD grid points. The data for the 13 SCH10 blocks with heat are shown in red, the data for the 88 SCH10 blocks without heat days are shown in gray.

In the composite for the WE region (Figure 12), the blocks are not co-located with the heat. RO200 and SCH10 identify the northern part of the ridge where the strongest GPH or PV anomalies are, while TM2D appears southeast of them. As TM2D detects the reversal of the meridional GPH gradient, it is expected that TM2D appears south of the highest GPH values. However, TM2D is southeast and not purely south or southwest of the highest GPH values. This position is favourable for WE heat days, because with the block to the southeast, the WE region lies in a region of warm-air advection from the southwest that supports the development of heat days.

The composites also show that TM2D appears least of all, RO200 more frequently, and SCH10 most often during WE heat days. The same observation is made when the JJA climatology is subtracted. However, the ORs show that even though SCH10 is most frequent, RO200 and TM2D increase the odds for heat more. Moreover, it is the blocks inside the WE region, especially in the southeastern edge of the WE region, that increase the odds for heat the most, and not the blocks shown in the composites. A strong, warm-air advection from the southwest can be expected if the blocks are in the southeastern edge of the WE region. This explains the spatial discrepancy of the blocks in the

composites in comparison to the heat-conducive blocks in the OR.

If a block is located upstream of the WE region, the WE region lies in the region of northerly winds, therefore in the region of cold-air advection. In other words, it makes sense that the ORs for all three indices are smaller than one in this region. If a block is located downstream of the WE region, than the WE region lies in a region of cyclones that feed the block (SHUTTS 1983) and therefore the conditions are unfavourable for WE heat days. This explains the ORs smaller than one downstream of the WE region. Finally, TM2D blocks in the Norwegian Sea reduce the odds of WE heat, possibly because the WE region again lies in a region of northerly/northeasterly winds and cold-air advection.

In short, from the analysis of the WE region we conclude that the choice of the blocking index determines the location of the blocks and the strength of the block-heat relation: While RO200 blocks increase the odds for co-located heat by a factor of 20, TM2D suggests an increase by a factor of 10, and SCH10 by a factor of 5 only. RO200 shows the highest increase due to its direct link to the thickness.

From the composites we know that SCH10 finds a block more often during WE heat days than the other indices. In terms of the OR equation (Equation 2), this means that the variable a is larger for SCH10 than for RO200 and TM2D. Nevertheless, the ORs in the WE heat region are smaller for SCH10 than for TM2D and RO200. One possible explanation for this observation is that the number of blocks without heat - i.e. the variable b in the OR equation (Equation 2) - is large for SCH10. Considering the number of blocks and the JJA climatology of the SCH10 index (Section 4.1) this explanation seems reasonable. This leads to the conclusion that only during a few SCH10 blocks does heat develop in the WE region, and that there are many SCH10 blocks without a WE heat signal.

One important difference between the SCH10 blocks with heat and SCH10 blocks without heat is the volumetric soil water content (Figure 13.e-f), which is low for episodes with heat. This is in agreement with the study of STEFANON et al. (2012), who found that summer maximum temperatures in the WE region are negatively correlated with co-located rainfall occurrence from January to May.

The SCH10 blocks with heat stay longer in the block region than the blocks without heat. A longer time in the block sector can help the WSDI to reach the heat-day threshold, if there is a positive temperature anomaly to the southwest that is advected into the WE region. The composites of the daily maximum temperatures (Figure 13.g-h) show that in most of the areas southwest of the WE region, the temperatures are higher for the blocks with heat than for the blocks without heat.

Another indication that the time in the block sector is important is the number of WSD grid points

in the WE region relative to the day the block enters the block sector (Figure 14.b). For the blocks with heat the number of WSD grid points steadily increase until they cross the threshold for a heat day when the block enters the block region. Such an increase cannot be observed for the blocks without heat. In other words, the blocks without heat probably move too fast to permit processes like warm-air advection to have an impact on temperature. It needs to be emphasized that the information that can be drawn from the analysis of the SCH10 blocks with and without heat is limited due to the small number of blocks with heat.

5 | Conclusions

In this thesis five different block detection indices were compared within the frame of European heat waves. The first index, TM2D, detects the meridional reversal of the GPH gradient at 500 hPa. The second index, RO200, detects a positive GPH anomaly at 200 hPa. The other three indices, SCH13/10/07, are variations of an index that detects a negative PV anomaly in the vertically-averaged (from 500 hPa to 200 hPa) PV (APV). The index SCH13 asks for an APV anomaly of -1.3 pvu, the index SCH10 for -1.0 pvu, and the index SCH07 for -0.7 pvu.

First the blocks identified by the five indices during summer (JJA) and on the northern hemisphere were compared. Second, the definition of an intensity threshold for the SCH index was investigated. Third, a number of European heat-wave case studies were analysed. Fourth, the blocking climatology during the heat days of different European regions in Europe were studied for the three selected blocking indices, TM2D, RO200, and SCH10. Finally, the differences between SCH10 blocks with heat and without heat in the western European (WE) region were addressed. Here a summary of the main findings and the most important results are given, followed by some ideas for possible extensions of the analyses.

The ambiguity regarding the detection of blocks was observed several times. From a climatological perspective the blocking indices differ with regard to the location, the frequency and the characteristics of the blocks they detect. The maximum JJA blocking-frequency grid points in the North Pacific reach 22% (SCH07), 18% (SCH10, TM2D), or 6% (SCH13, RO200). SCH13/10/07, but not RO200 or TM2D, detect a second JJA blocking-frequency maximum in the North Atlantic. TM2D shows two latitudinal bands of JJA blocking frequency maxima, while the other indices show only one. Compared to the other indices, SCH07 detects large and long-living; TM2D and SCH10 many; RO200 few, large and short-living; and SCH13 small and short-living JJA blocks.

From the perspective of single European heat-wave case studies, the indices differ with regard to the detection, location, and the size of the blocks. In the cases of 1994, 2003, and 2015, four of the five indices detect a block. In the cases of 2006 and 2013, the three indices TM2D, SCH10, and SCH07 find

a block. In the case of 2007, only TM2D and SCH07 identify a block. Often TM2D appears spatially shifted from the other indices. In all case studies RO200 and SCH10 identify the largest blocks and show the largest overlap with the heat area.

From the perspective of the heat-wave climatologies, the three indices TM2D, RO200, and SCH10 differ - mainly for the western European (WE) region, but also in part for the Scandinavian (SC) region - with regard to the blocking frequency and strength of the block-heat relation. The maximum blocking frequencies observed on individual grid points during heat waves reach 40% (SCH10), 30% (TM2D), or 15% (RO200) for the SC region; and 30% (SCH10), 15% (RO200), or 10% (TM2D) for the WE region. For the WE heat waves, the indices detect the blocks either north (RO200, SCH10) or east (TM2D) of the WE region. The few blocks in the WE region increase the odds of a heat wave by a factor of 20 (RO200), 10 (TM2D), or 5 (SCH10).

The observations just described emphasize the differences between the five indices. However, agreements between the five indices were also found. All five show a maximum JJA blocking frequency in the North Pacific. All five detect a block in the case study of 2010. The four indices RO200, SCH13, SCH10 and SCH07 detect the blocks at roughly the same location in the case studies and in the JJA climatology. During SC heat waves, the three indices used detect the blocks co-located with the heat, and agree that these blocks increase the odds for a SC heat day by a factor of 10. For the SC and the WE region, the three indices detect the blocks that provide favourable and unfavourable conditions for heat waves at the same locations.

Another insight is that some of the indices may be inappropriate for use for certain purposes. RO200 should not be used to assess the relation between blocks and heat at different latitudes, because it always finds a stronger relation in the south than in the north, due to its link to absolute temperatures. TM2D and SCH07 should not be used at low latitudes, because they erroneously detected subtropical high-pressure systems that are not in a classical sense blocks, as seen in the case study of 2007. The three indices SCH13/10/07 should not be used during all seasons of the year, because the choice of the intensity threshold directly determines at which latitudes blocks can be detected. For instance, at 40°N, 5% of the APV' values are below -0.7 pvu, while 0% are below -1.3 pvu. Because the westerlies, and with this also the blocking anticyclones, are further south in summer than in winter, one might suggest using a higher intensity threshold in summer than in winter.

Generally, this research has indicated that the use of SCH07 as a blocking index is particularly problematic. Besides the erroneously detected subtropical high-pressure systems, the size and lifetime

distributions of the JJA blocks indicate that SCH07 detects blocks very generously compared to the other indices. Moreover, the intensity threshold used for SCH07 corresponds to the lowest 14% of the extratropical JJA distribution of the anomalous APV (APV'). This is rather high compared to the thresholds of SCH10 and SCH13, which correspond to the lowest 6% and 3%. In addition, the higher the APV' threshold, the larger the fraction of APV' values below the threshold per latitude that are classified as blocks: 90% (-0.7 pvu), 77% (-1.0 pvu), and 62% (-1.3 pvu).

Finally, some process understanding was gained in the analysis of SCH10 blocks with and without heat in the WE region. It was shown that the blocks with heat are more stationary than the blocks without heat. In addition, low volumetric soil water content in the WE region and high absolute temperatures southwest of the WE region were identified to support the development of heat in the WE region.

All this provides an overview of the behaviour of different blocking indices during European heat waves. The research could be further extended by testing whether the patterns observed in the composites of the block-heat relation analysis differ significantly from the climatology; considering more blocking indices; using different datasets instead of ERA-interim alone; and analysing more case studies and regions, for example. Additionally, other heat indices could be tested, as the WSDI based on a linear detrended temperature field may not be the optimal choice.

Appendix

A.1 Supplementary Material - Literature Review

A.1.1 Review Blocking Indices

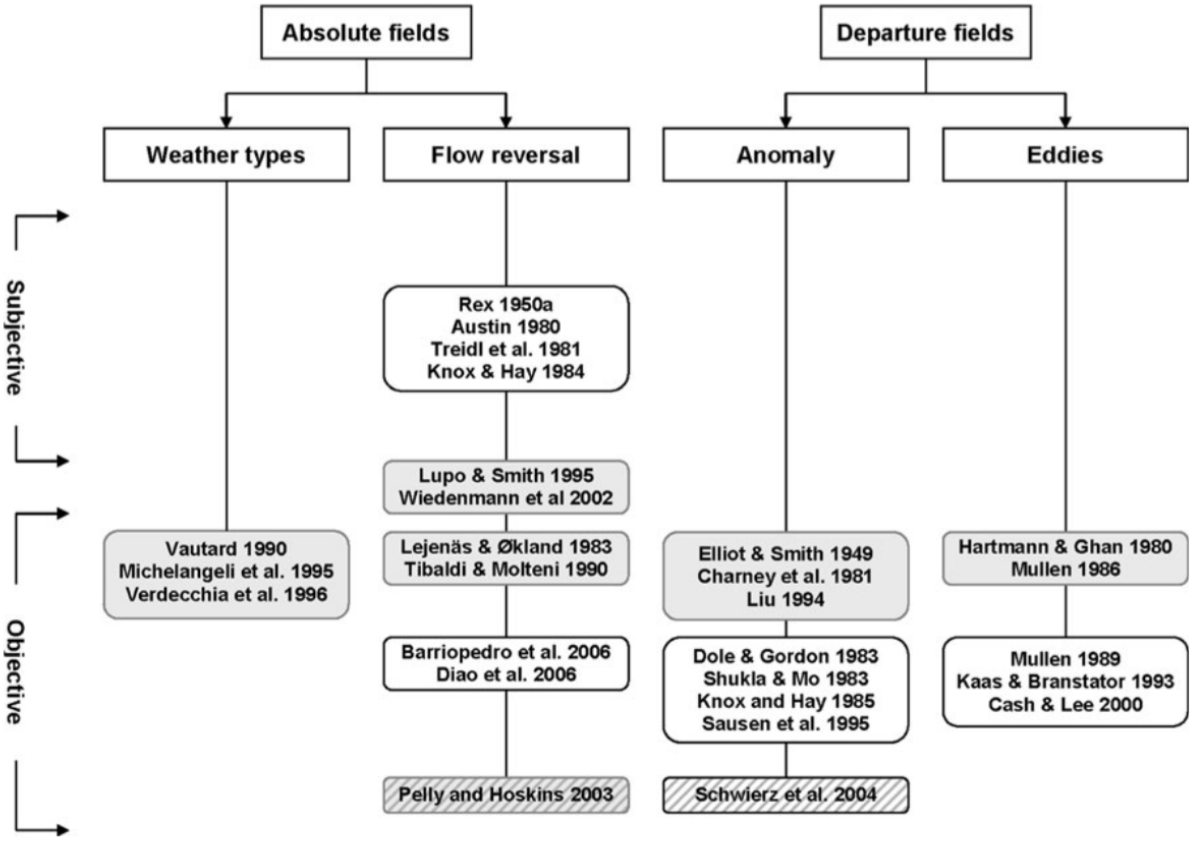

Figure A1: Review of the block detection methods by BARRIOPEDRO et al. (2010). The methods are sorted according to their objectivity (left rows), base field (header columns), and specific blocking index (subheader columns). The methods based on one dimension (two dimensions) are shaded (not shaded). The methods using dynamical (standard isobaric) variables are dashed (not dashed).

A.1.2 Geopotential Height

The geopotential (Φ) is defined as the work that must be done against the Earth's gravitational field to lift a mass of 1 kg from sea level to a given altitude in the atmosphere. Thus, Φ at a given height z corresponds to (WALLACE and HOBBS 2006, MARTIN 2006):

$$\Phi(z) = \int_0^z g \, \mathrm{d}z \tag{A1}$$

Φ = geopotential (J kg^{-1} or m^2 s^{-1})

g = gravitational acceleration (m s^{-2})

Through dividing Φ by the gravitational constant g_0, one receives the quantity geopotential height (GPH):

$$GPH = \frac{\Phi(z)}{g_0} = \frac{1}{g_0} \int_0^z g \, \mathrm{d}z \tag{A2}$$

GPH = geopotential height (gpm)

g_0 = gravitational constant (m s^{-2})

Near the surface - where g is close to g_0 - the geometric height and GPH are approximately at the same altitude. Further up in the atmosphere - where g is smaller than g_0 - the geopotential meter becomes bigger than the geometrical meter; because, with the same amount of work one can move 1 kg over a larger distance.

In meteorology GPH is often used to describe the height of a given pressure level. Thus, regions of high pressure (i.e. also blocks) are regions of positive anomalies in the GPH field at a certain hPa level. A link to absolute temperatures can be drawn when the difference between two GPH fields is considered, the so-called thickness (h) (WALLACE and HOBBS 2006):

$$h = GPH_2 - GPH_1 = \frac{R_d}{g_0} \int_{p_2}^{p_1} T_v \frac{\mathrm{d}p}{p} \tag{A3}$$

GPH_1 and GPH_2 = geopotential height at p_1 and p_2 (gpm)

p_1 and p_2= pressure levels (Pa)

R_d= gas constant for dry air (J kg^{-}1 K^{-}1)

T_v= virtual temperature (K)

g_0 = gravitational constant (m s^{-2})

From Equation A3 we can see that h is larger for warm air masses than for cold air masses. In the same manner, high values of h are easier reached in low latitudes were absolute temperatures are higher than in high latitudes.

A.1.3 Ertel Potential Vorticity

Ertel Potential vorticity (PV) can be derived from the full primitive equations. If friction and diabatic processes are neglected, PV is defined as the product of the absolute vorticity (η) and the 3-dimensional gradient of potential temperature ($\nabla\theta$):

$$PV = \frac{1}{\rho}\eta\nabla\theta \tag{A4}$$

PV = potential vorticity (pvu or 10^{-6} m^2 s^{-1} K kg^{-1})

ρ = density (kg m^{-3})

η = absolute vorticity vector (s^{-1})

θ = potential temperature (K)

PV and θ are conserved for adiabatic and frictionless motion. Therefore, an air parcel moving along a surface of constant θ will keep its PV as long as diabatic processes and friction are negligible; i.e. are dominated by advective processes. This principle is called the Lagrangian conservation principle and implies that PV on isentropic surfaces (IPV maps) can be used to trace air masses (HOSKINS 1985).

Given a balance condition (e.g. geostrophic balance) and appropriate boundary conditions (surface θ-distribution), the PV distribution is sufficient to diagnostically determine all other dynamical variables, i.e. the three wind components, temperature distribution, GPH, and static stabilities. This so-called PV invertibilty principle applies also if diabatic and frictional processes are involved (HOSKINS 1985). In the context of blocks, one can use the invertibility principle to relate anticyclones to negative PV anomalies.

A.2 Supplementary Material - Data and Methods

A.2.1 Heat Indices

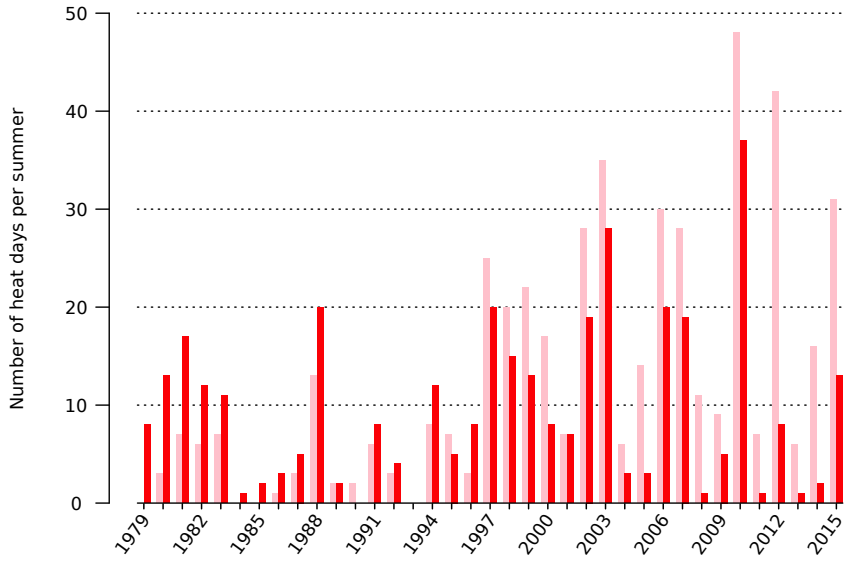

Figure A2: Sum of European heat days (at least 5 × 5 land-grid points report a warm spell day within the region reaching from 30°W to 55°E and 30°N to 80°N) for each summer from 1979 to 2015. The sum for the warm spell day index with the original ERA-interim two meter temperature, the 90th calendar-day percentile, and 6 consecutive days is shown in pink. The sum for the warm spell day index with the linear-detrended ERA-interim two meter temperature, the 90th calendar-day percentile, and 6 consecutive days is shown in red.

Table A1: Linear trend of the time series of the sum of heat days (at least 5 × 5 grid points report a warm spell day within the region reaching from 30°W to 55°E and 30°N to 80°N) per summer for the WSDI with trend and without trend. The coefficient b of the linear model $y(x) = a + b \times x$ is estimated and the p-value of the F-statistic for b is given. If the trend is found to be significant at the level $\alpha = 0.1\%$, the p-value is marked with ***.

WSDI	with trend	without trend
b	0.73	0.08
p-value	$4.02 \times 10^{-5***}$	0.55

A.2.2 Blocking Indices

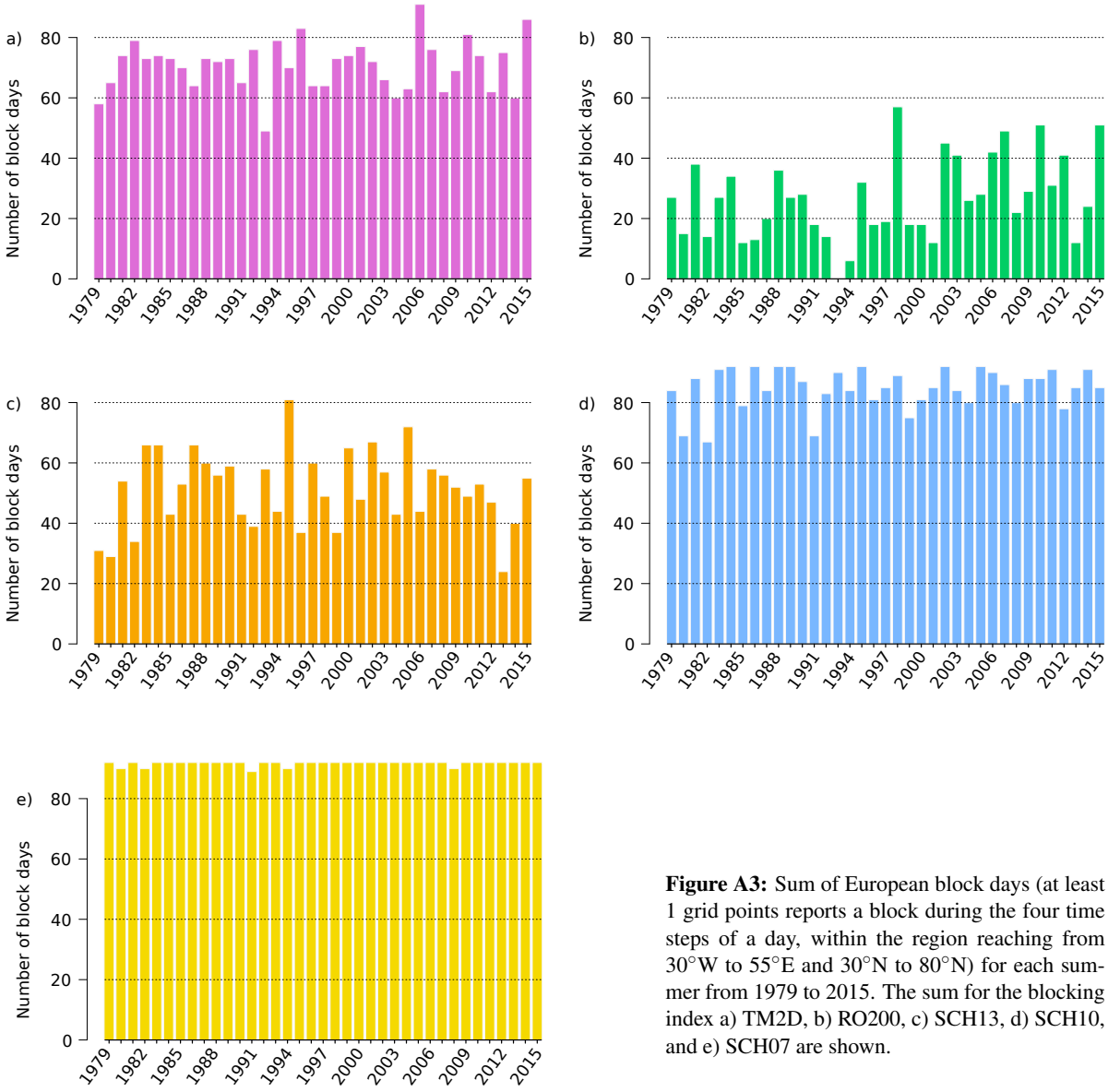

Figure A3: Sum of European block days (at least 1 grid points reports a block during the four time steps of a day, within the region reaching from 30°W to 55°E and 30°N to 80°N) for each summer from 1979 to 2015. The sum for the blocking index a) TM2D, b) RO200, c) SCH13, d) SCH10, and e) SCH07 are shown.

Table A2: Linear trend of the time series of the sum of European block days (at least 1 grid point reports a block during the four time steps of a day, within the region reaching from 30°W to 55°E and 30°N to 80°N) per summer for the five blocking indices. The coefficient b of the linear model $y(x) = a + b \times x$ is estimated and the p-value of the F-statistic for b is given. If the trend is found to be significant at the level $\alpha = 5\%$, the p-value is marked with *.

Index	TM2D	RO200	SCH13	SCH10	SCH07
b	0.08	0.45	0.01	0.11	0.02
p-value	0.54	0.03^*	0.97	0.3	0.2

A.2.3 Temperature Sensitivity of RO200

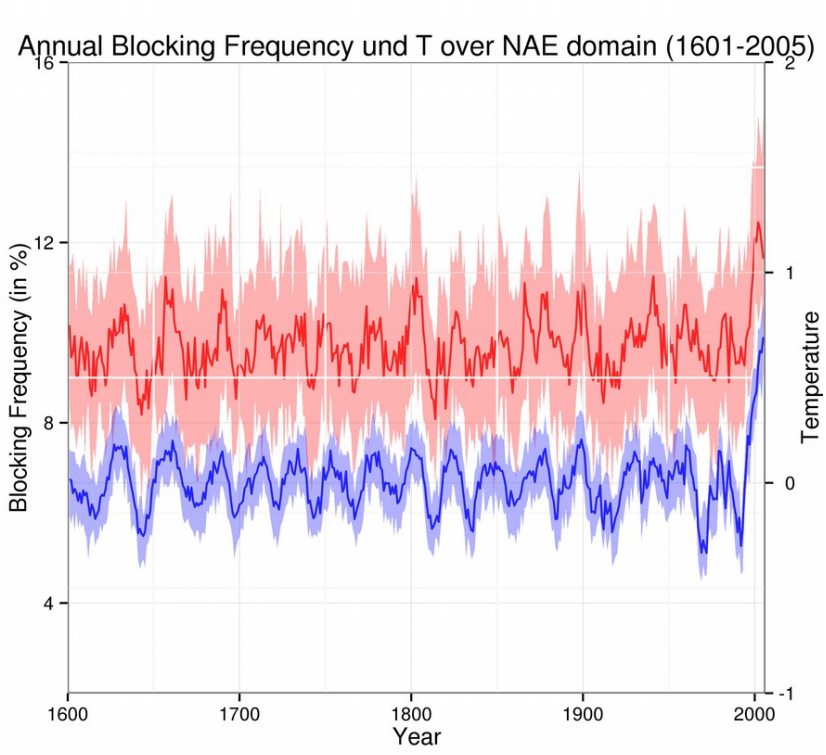

Figure A4: Blocking frequencies (red) of the index RO200 and the temperature anomaly (blue) relative to the running 30-years mean over the North Atlantic and European (NAE) domain. The thick line represents the median of the 30 ccc400 models and the shaded area represents the range of the 10 to 90 percentiles. Figure is taken from ROHRER (2017b).

A.3 Supplementary Material - Block Characteristics

A.3.1 Blocking Frequencies

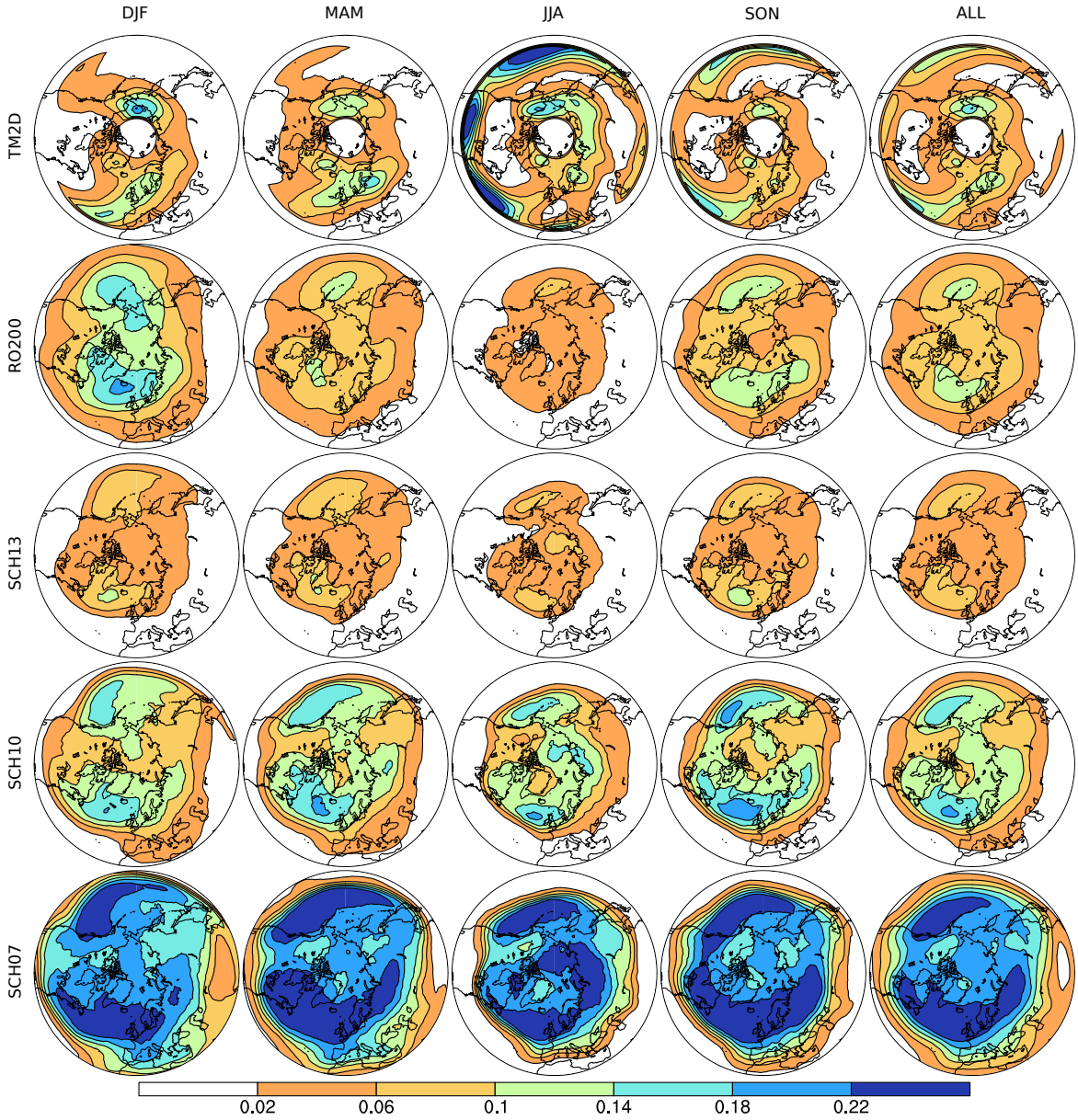

Figure A5: Northern hemispheric blocking frequency of the block detection indices TM2D (first row), RO200 (second row), SCH13 (third row), SCH10 (fourth row), and SCH07 (fifth row) for the winter (first column), spring (second column), summer (third column), autumn (fourth column) and over the period from 1979 to 2015.

A.3.2 Numbers and Lifetimes

Table A3: Number and mean lifetime of the blocks found by each block detection index during each season of the year and within the period from 1979 to 2015.

Index	DJF	MAM	JJA	SON
TM2D	433 (8.7 d)	543 (8.6 d)	941 (9.4 d)	588 (8.1 d)
RO200	382 (12 d)	406 (9 d)	325 (8.4 d)	425 (10.6 d)
SCH13	451 (9.4 d)	642 (9 d)	679 (8.5 d)	669 (8.7 d)
SCH10	708 (12.2 d)	793 (12.3 d)	868 (12.4 d)	768 (12.3 d)
SCH07	474 (18 d)	344 (18.2 d)	357 (17 d)	339 (18.9 d)

A.4 Supplementary Material - Threshold Choice

A.4.1 Seasonal Thresholds

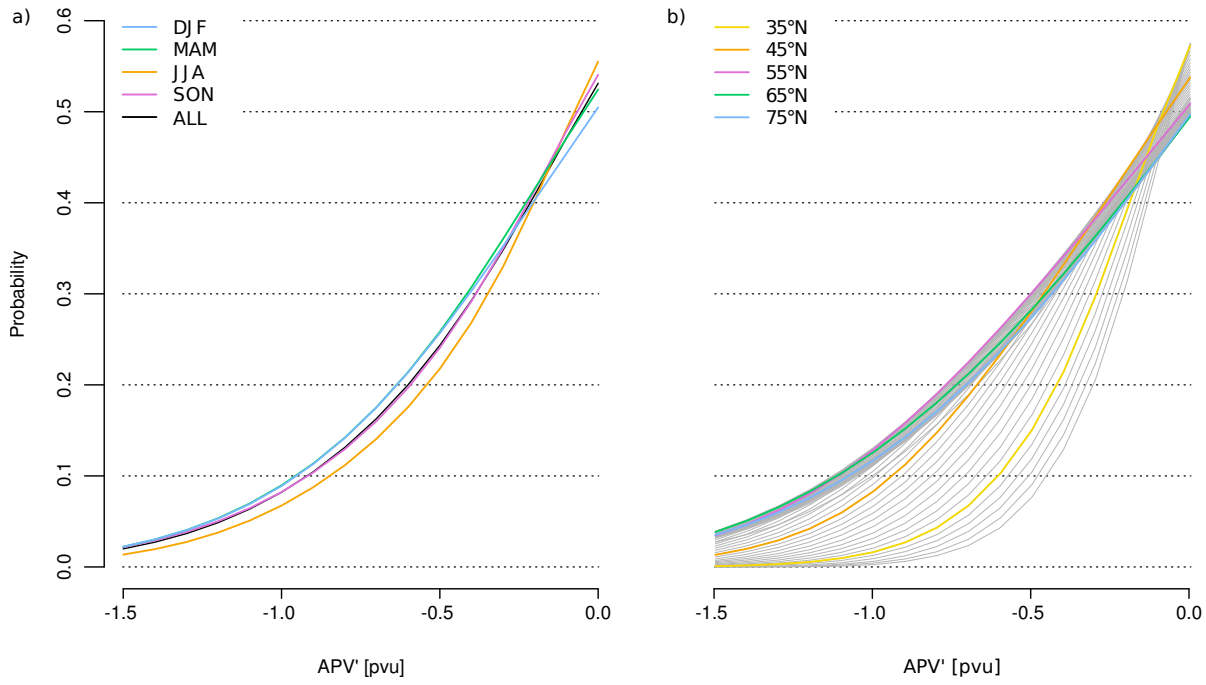

Figure A6: a) Probability (y-axis) of the APV' values north of 30°N and of various season and the whole year to be smaller than a given threshold (x-axis). b) Probability (y-axis) of the APV' values of each latitude from 30°N northwards to be smaller than a given threshold (x-axis). Only the APV' values from 1979 to 2015 are considered.

A.5 Supplementary Material - Case Studies

A.5.1 Case Study 2006

The heat wave in July 2006 affected central Europe (RUSSO et al. 2015), more precisely Switzerland, France, Poland, Belgium and the Netherlands (REBETEZ et al. 2009). REBETEZ et al. (2009) linked the heat in July 2006 to a persistent anticyclone within an omega block lasting from July 15th to 27th 2006.

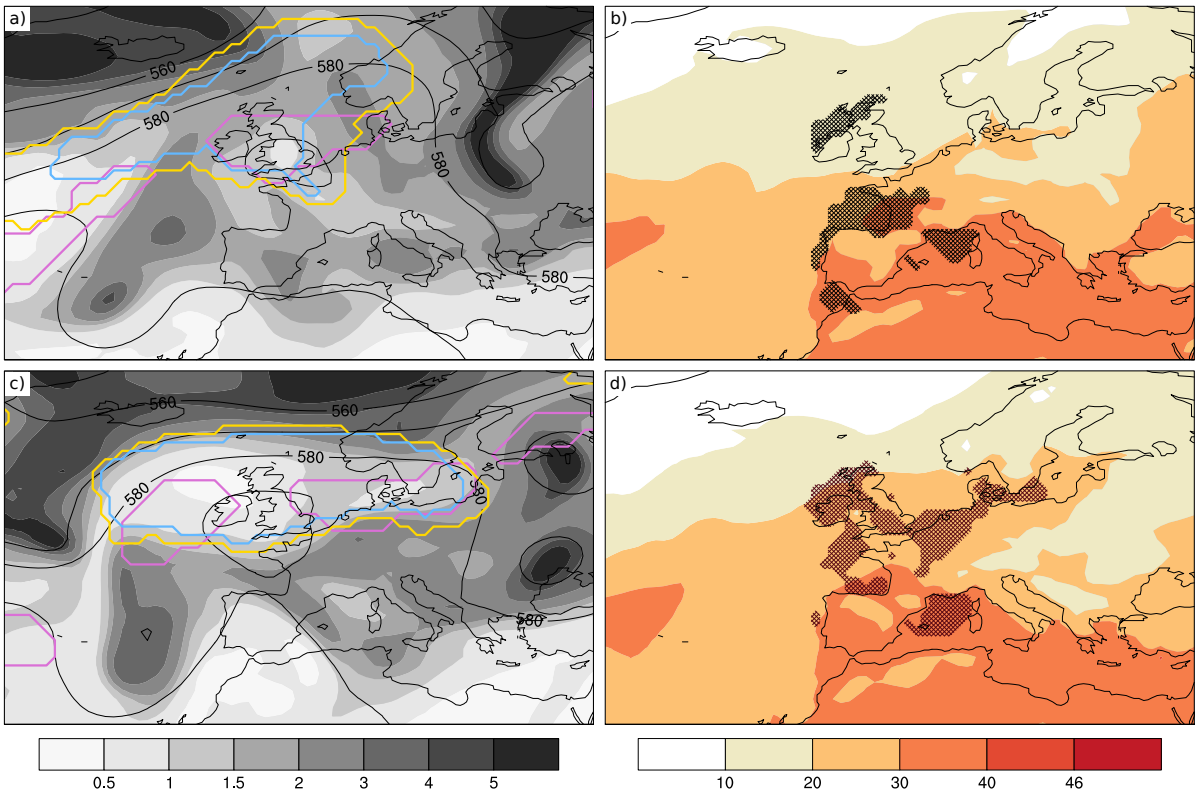

Figure A7: Same as Figure 7 but for a)-b) July 15th at 12 UTC, and c)-d) July 17th 2006 at 12 UTC.

A.5.2 Case Study 2013

The UK Met Office reported a heat wave in the United Kingdom from July 3th to 23th 2013 METOFFICE (2016) with the highest temperatures since 2006. In a similar way, the Irish weather service Met Éireann summarizes the period from July 5th to 21st 2013 as very dry and warm with several stations reporting drought conditions METÉIREANN (2013).

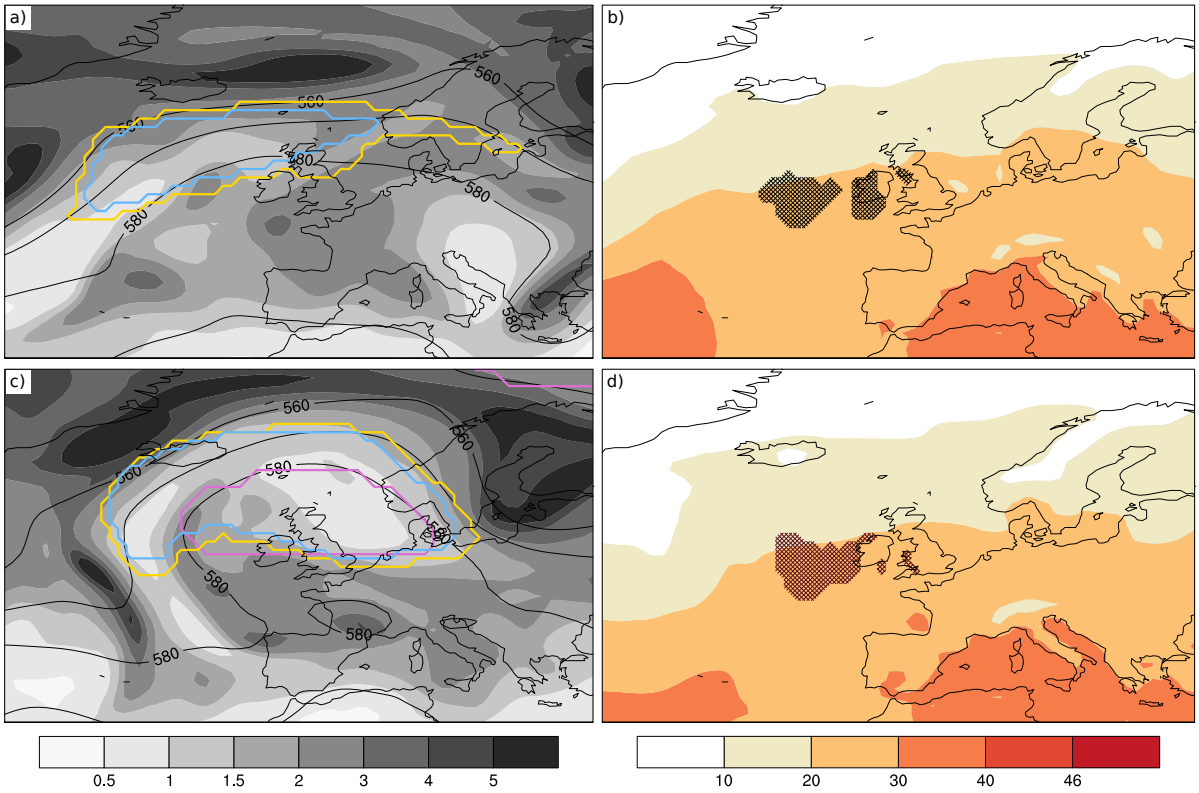

Figure A8: Same as Figure 7 but for a)-b) July 17 at 12 UTC, and c)-d) July 19th 2013 at 12 UTC.

A.5.3 Case Study 2015

In July and August 2015 Switzerland experienced three heat waves. The first one from July 1st to 7th, and the second one from July 16th to 24th, and a last short one from August 5th to 9th. On July 7th the meteorological station in Geneva recorded a temperature of 39.7°C, the highest value since the beginning of measurements in 1864 (METEOSCHWEIZ 2016). METEOSCHWEIZ (2016) concluded that a strong ridge and dry soil conditions contributed to the first heat wave.

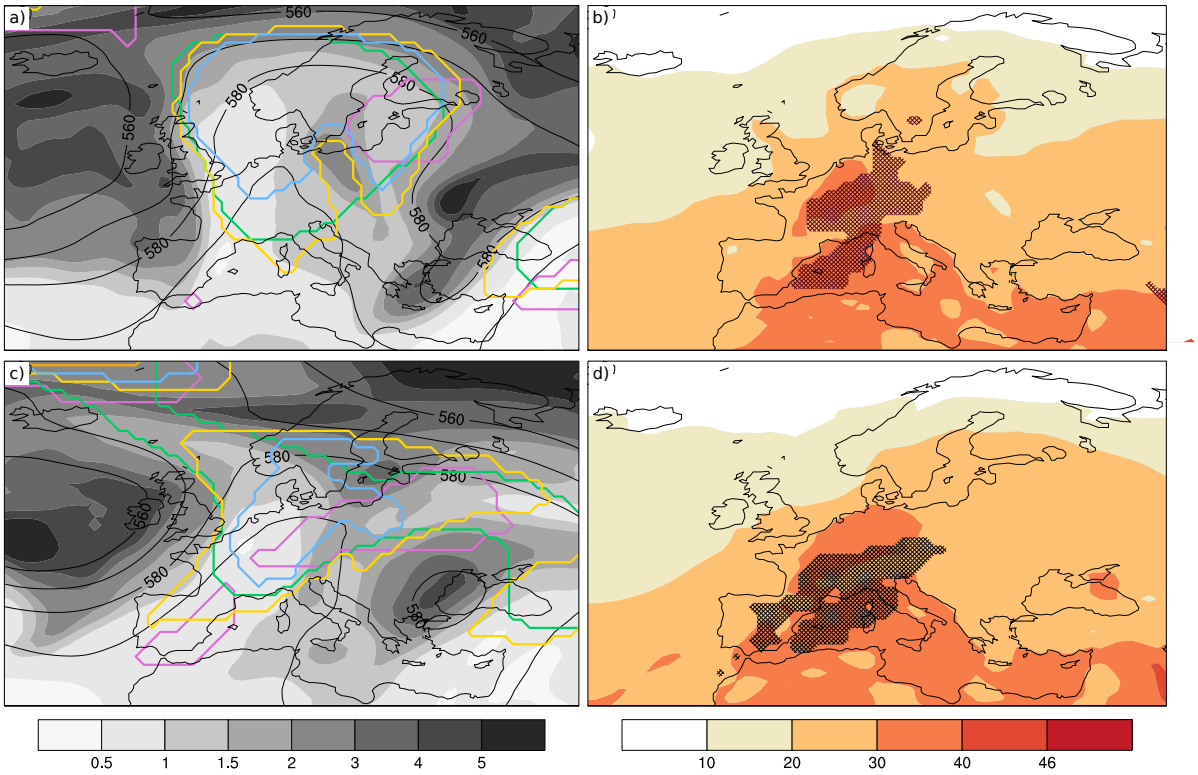

Figure A9: Same as Figure 7 but for a)-b) July 2nd 2015 at 12 UTC, and c)-d) July 4th 2015 at 12 UTC.

A.6 Supplementary Material - Blocks and Heat

A.6.1 Heat Regions

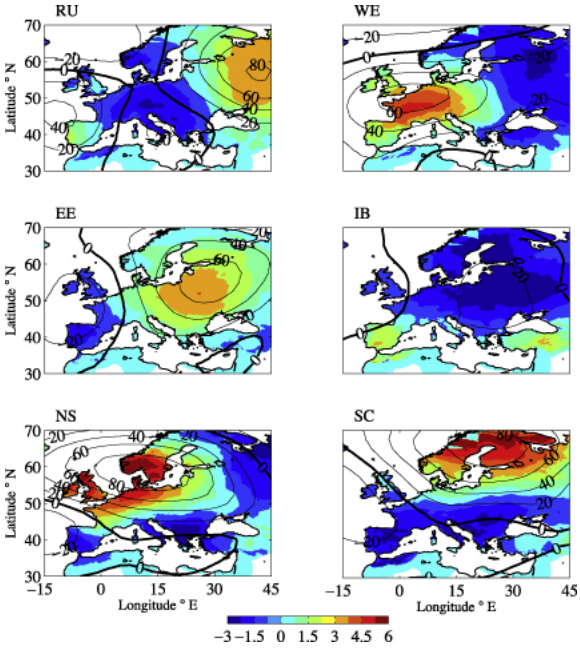

Figure A10: Heat regions identified by STEFANON et al. (2012) who conducted a hierarchical clustering of heat event maps.

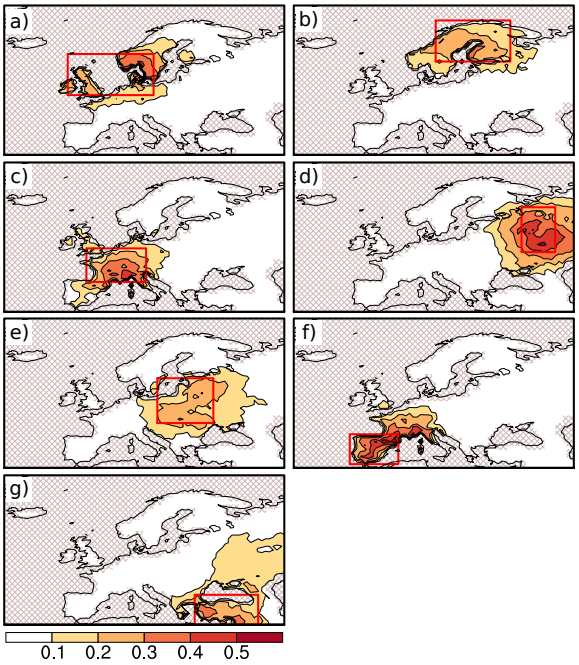

Figure A11: Composites of the WSDI during the heat days of the seven heat regions a) North Sea, b) Scandinavia, c) western Europe, d) Russia, e) eastern Europe, f) Iberian Peninsula, and g) southeastern Europe.

A.6.2 Heat Events

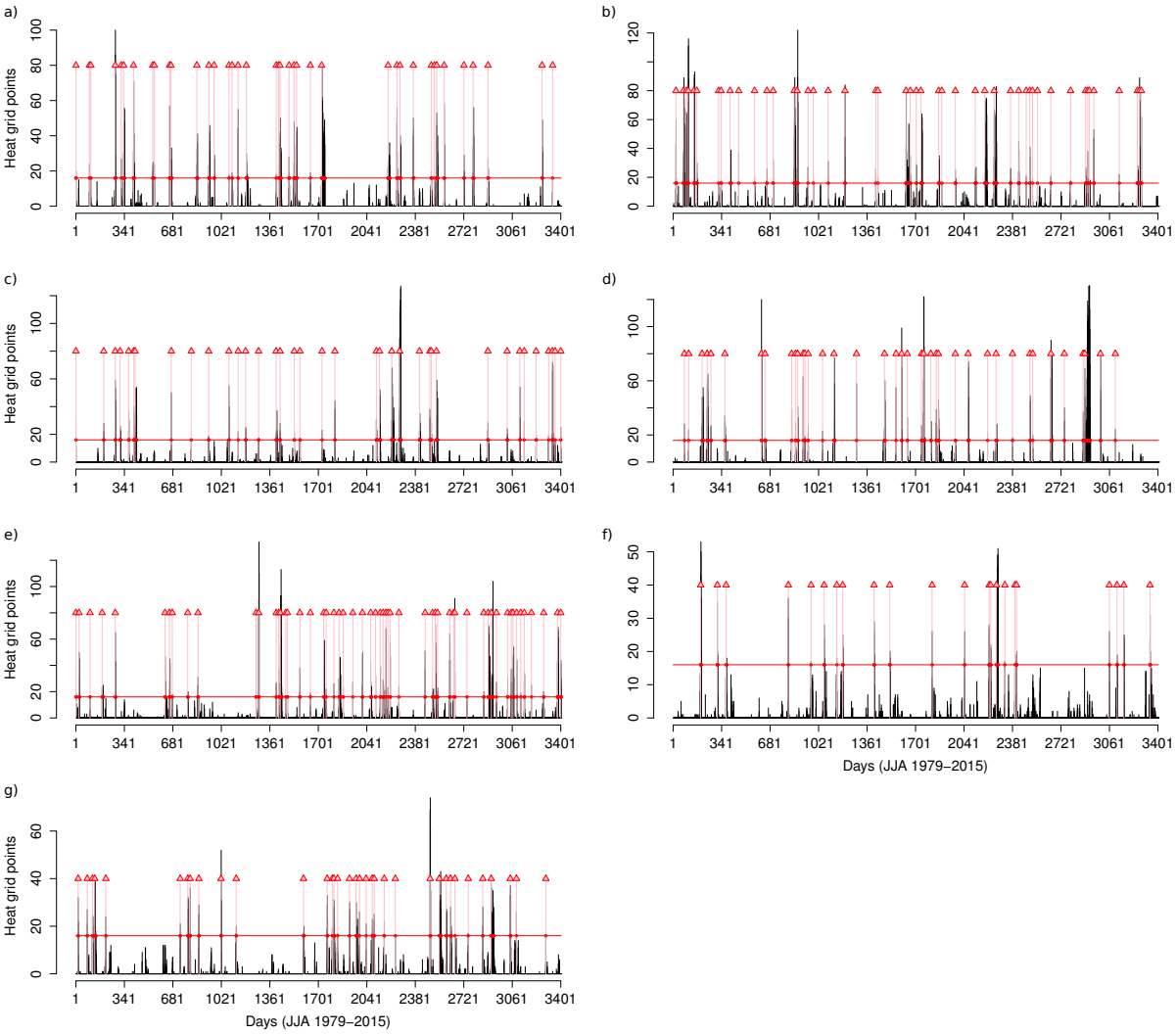

Figure A12: Number of heat event in the period JJA 1979-2015 for each of the seven heat regions a) North Sea, b) Scandinavia, c) western Europe, d) Russia, e) eastern Europe, f) Iberian Peninsula, and g) southeastern Europe. The black bars show the number of WSD grid points per day, the red horizontal line is the heat day threshold (16 WSD grid points), the red vertical lines with a triangle at the top show all heat event (heat day separated 7 days from the preceding heat day) onsets.

A.6.3 Composites and Odds Ratios

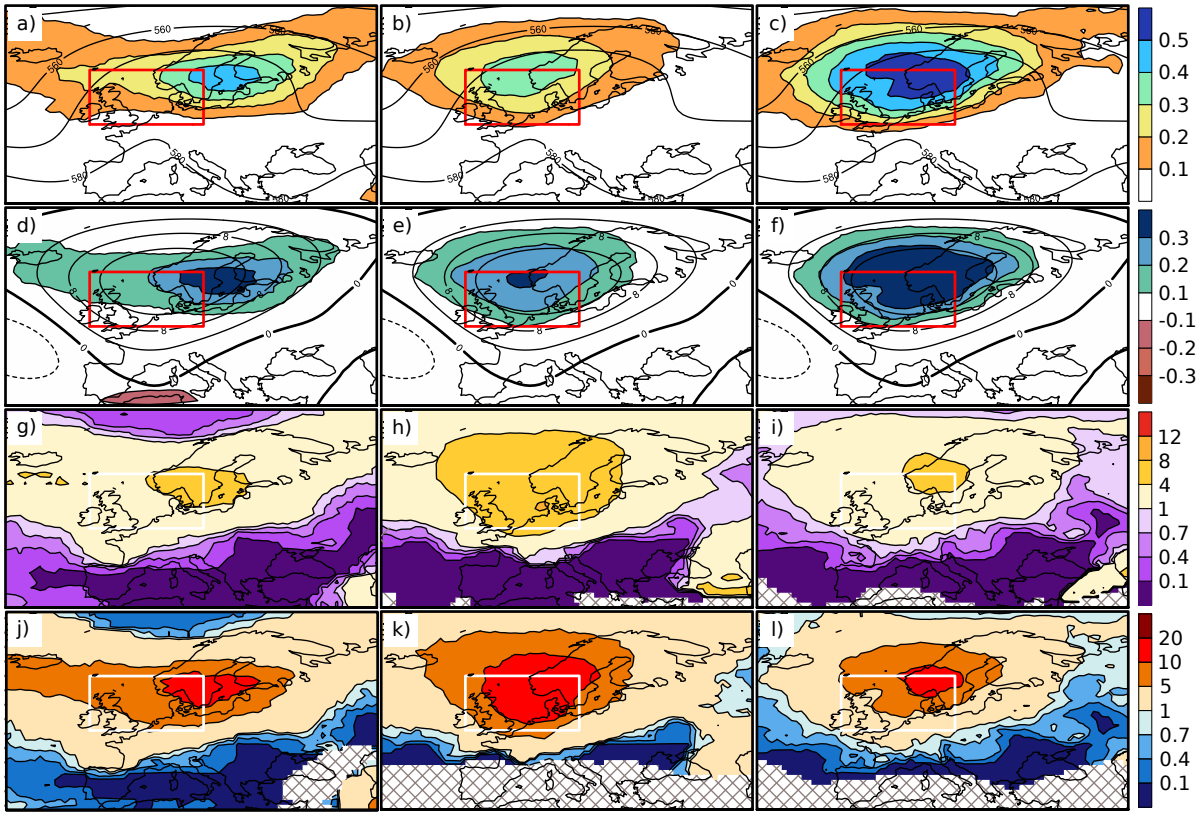

Figure A13: Top: Composites during heat days in the North Sea region (8°W to 15°E, and 51°N to 62°N) of the blocking fields (shading) and of the GPH at 500 hPa (black contours) are shown in a) TM2D, b) RO200, and c) SCH10. Upper middle: The blocking frequency anomaly of a), b), c) relative to the JJA blocking climatology (1979 to 2015) are shown in d) TM2D, e) RO200, and f) SCH10. The black contours in d), e), f) are GPH anomalies at 500 hPa relative to the JJA climatology in 4 hPa intervals, the thick line denotes 0 hPa, dashed lines denote negative anomalies, and thin lines positive anomalies. Lower middle: The blocking frequency of a), b), c) divided by the JJA blocking climatology (1979 to 2015) are shown in g) TM2D, h) RO200, and i) SCH10. Bottom: The odds ratio between SC heat days with blocks and SC heat days without blocks is shown in j) TM2D, k) RO200, and l) SCH10. The red/white framed box represents the heat region. The regions where the JJA blocking climatology (1979 to 2015) of the individual blocking index is smaller than 0.005 are masked out. The maps show the European domain (25° W to 50° E, and 35° N to 75° N).

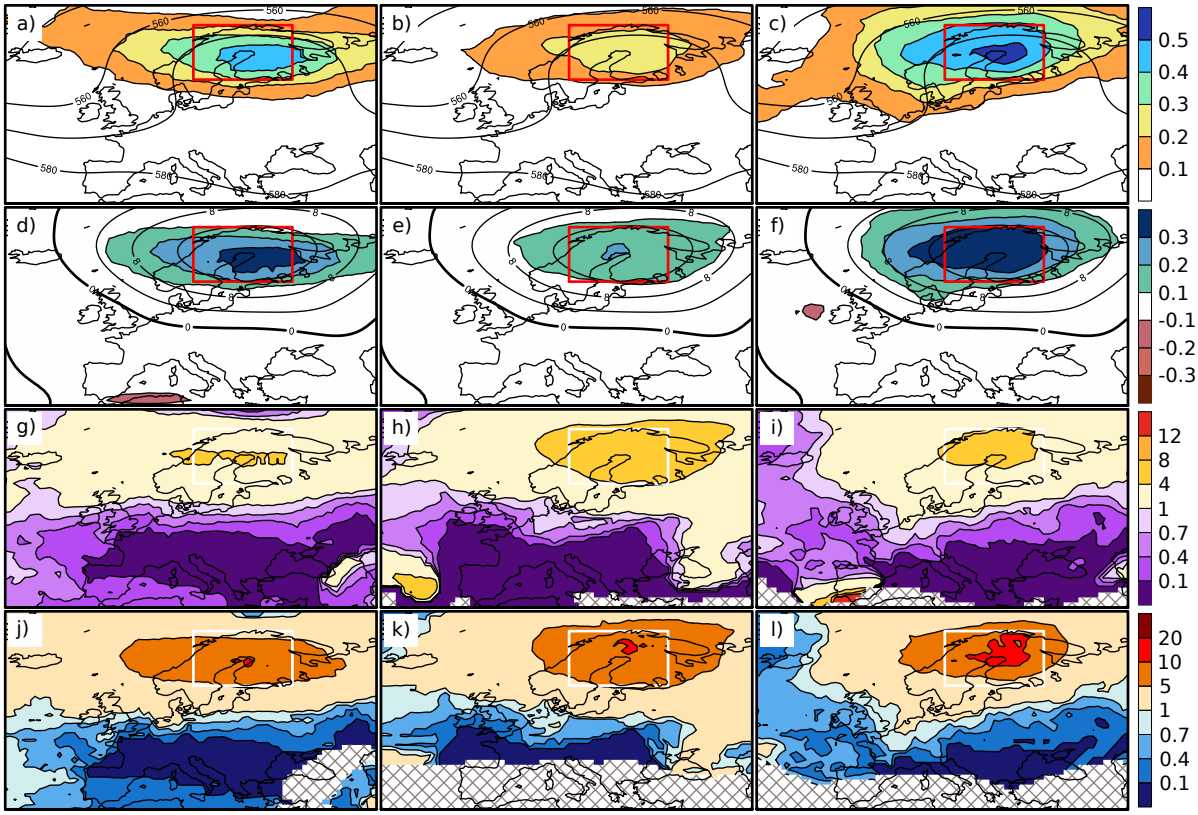

Figure A14: Same as Figure A13 but for the Scandinavian region (13°E to 33°E, and 60°N to 71°N).

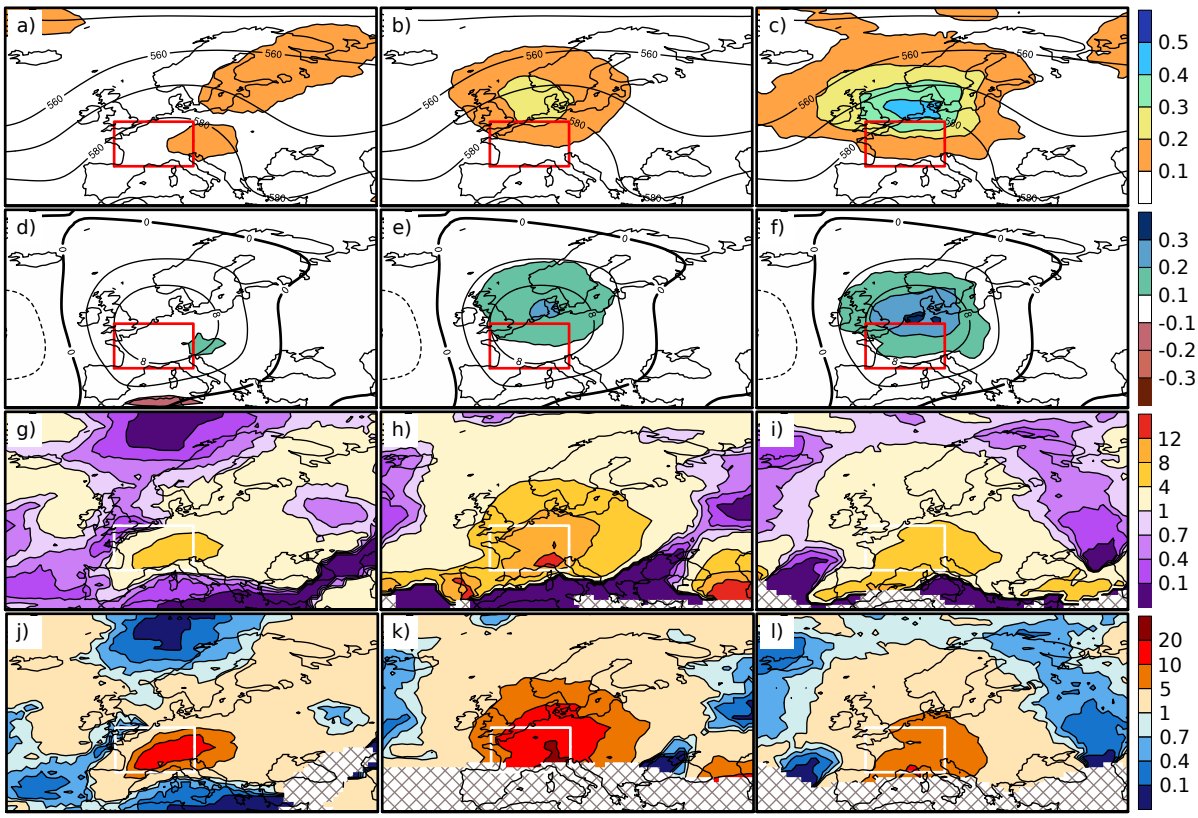

Figure A15: Same as Figure A13 but for the western European region (3°W to 13°E, and 43°N to 52°N).

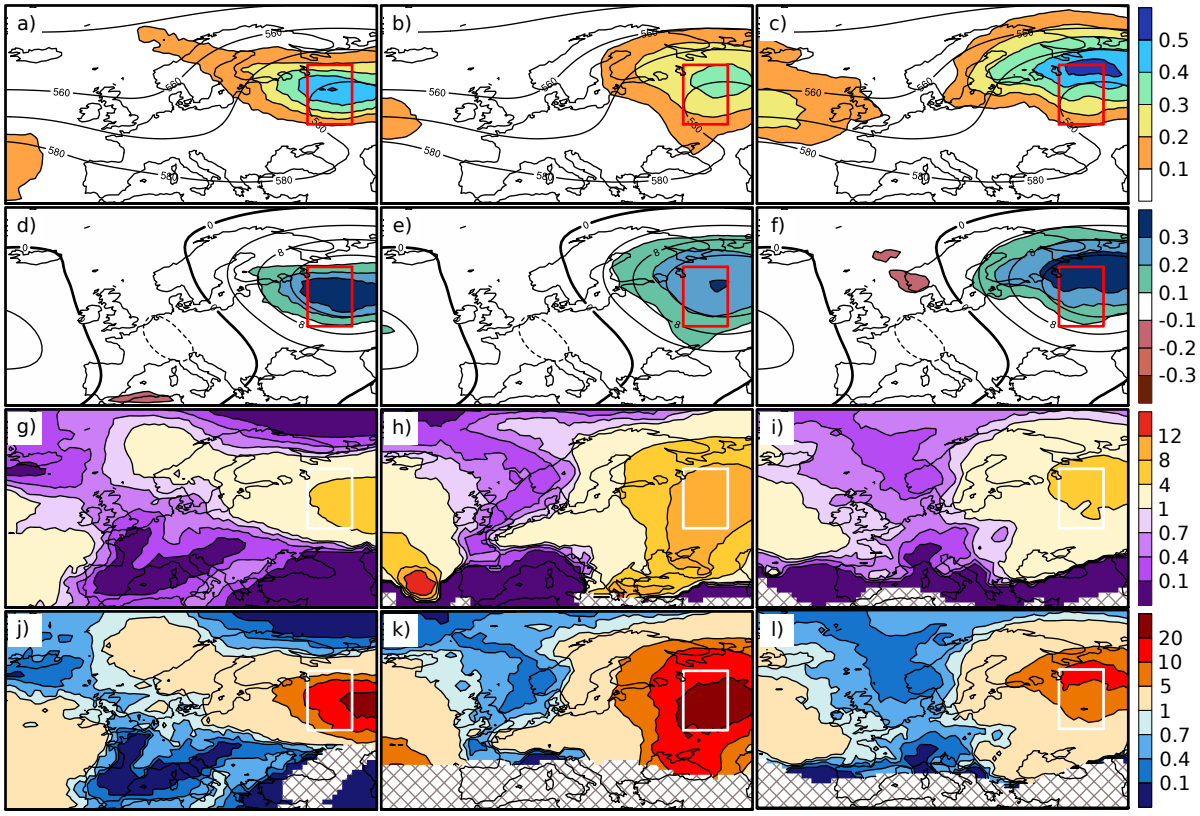

Figure A16: Same as Figure A13 but for the Russian region (36°E to 45°E, and 51°N to 63°N).

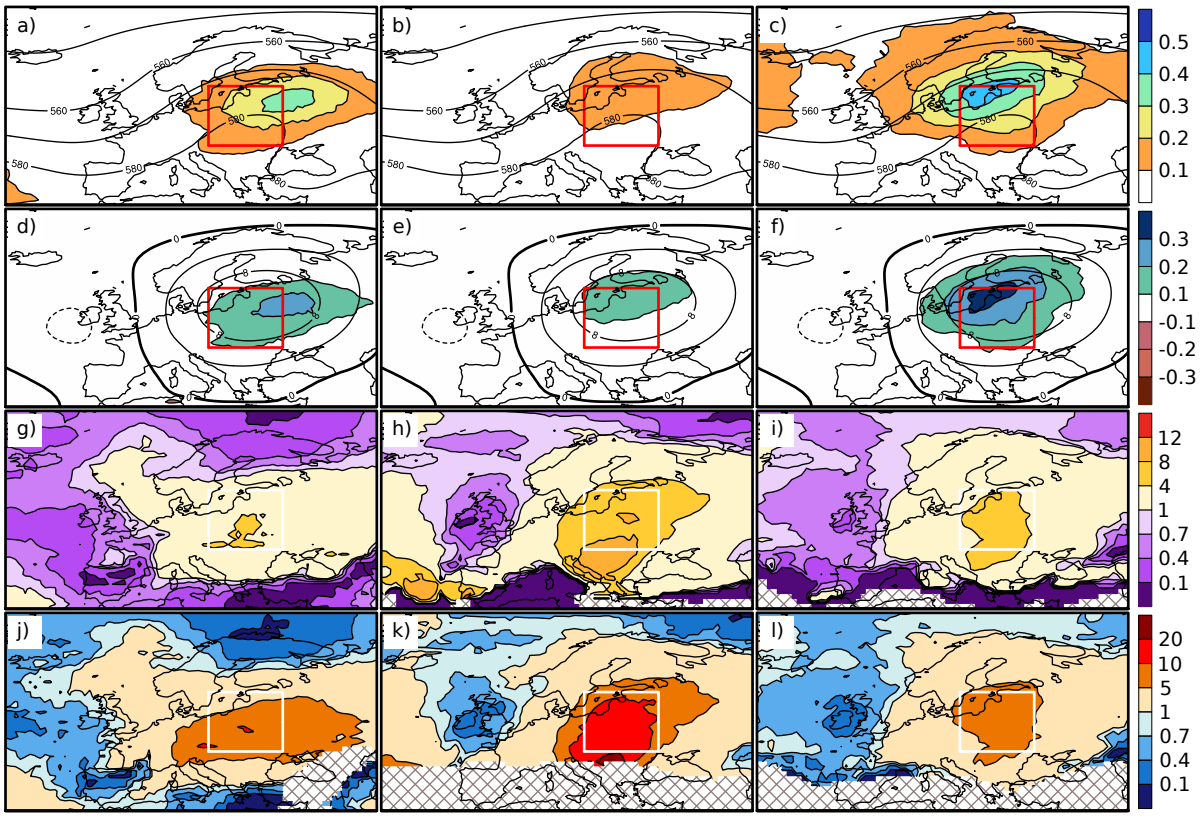

Figure A17: Same as Figure A13 but for the eastern European region (16°E to 31°E, and 47°N to 59°N).

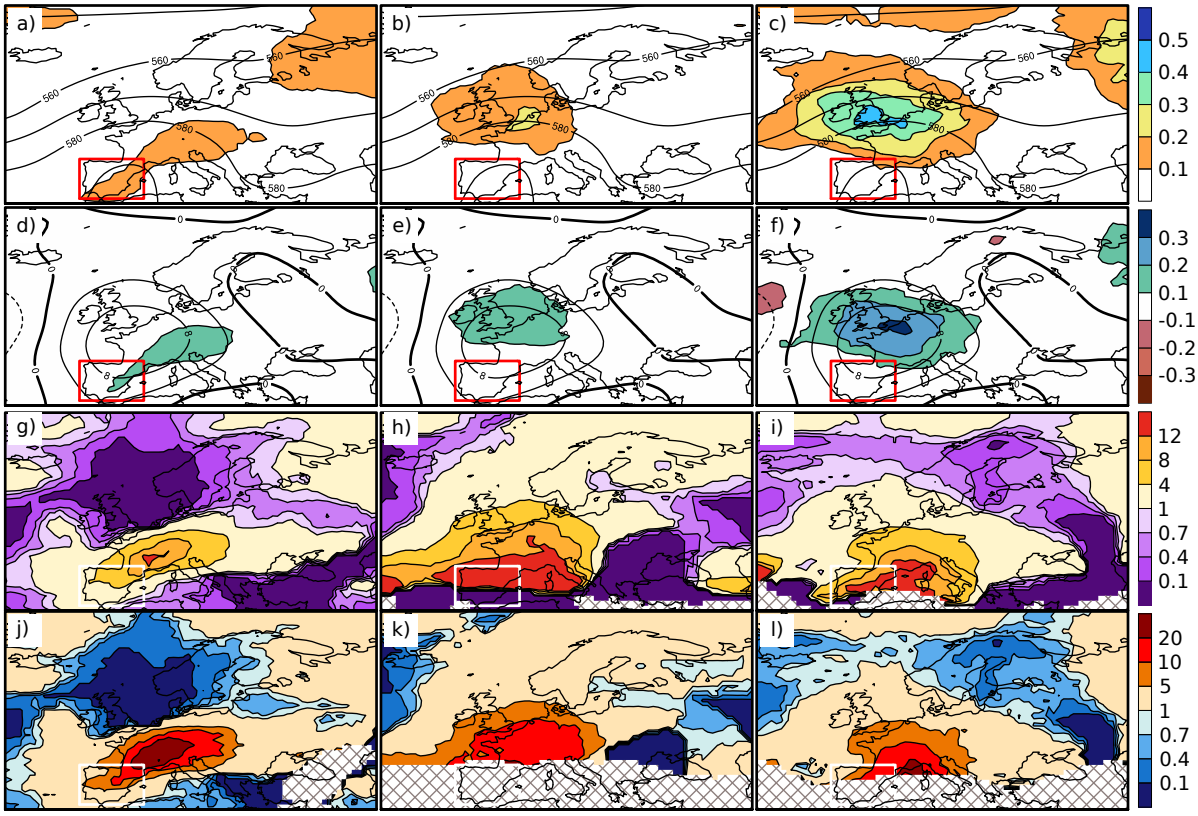

Figure A18: Same as Figure A13 but for the Iberian Peninsula region (8°W to 15°E, and 51°N to 62°N).

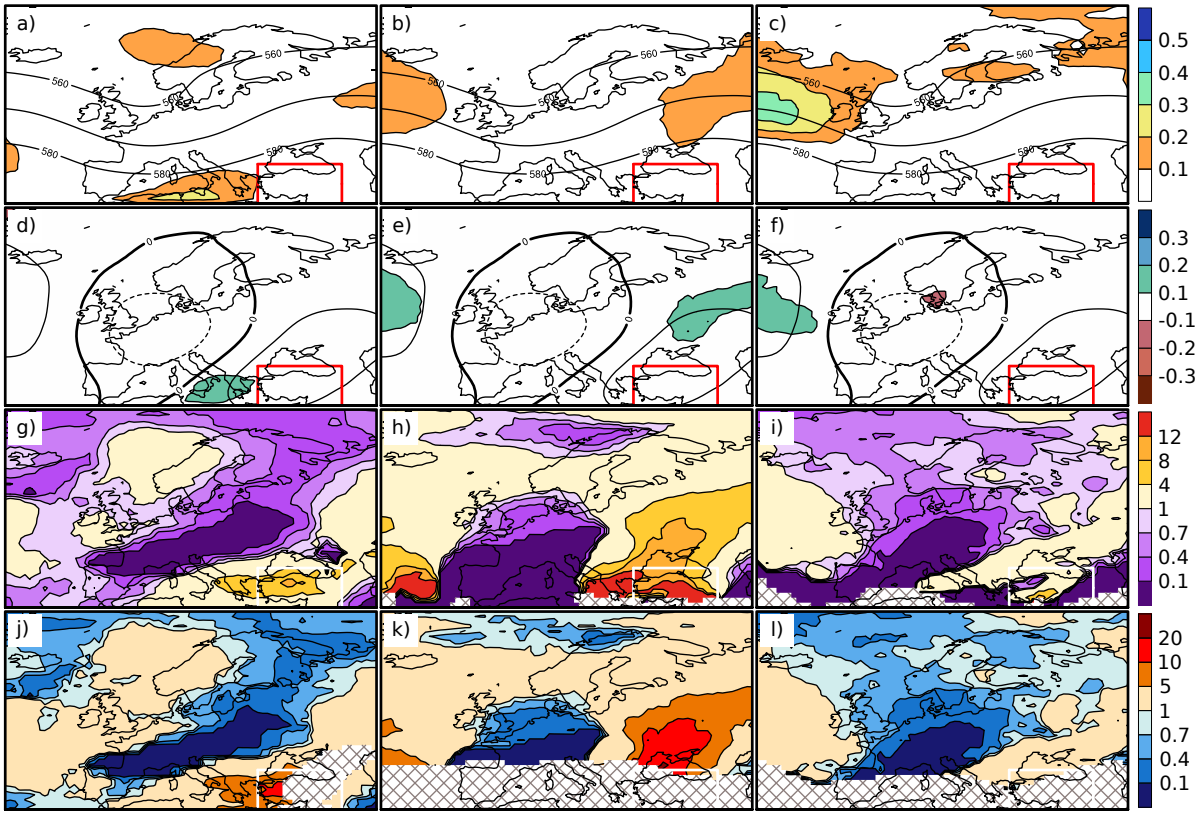

Figure A19: Same as Figure A13 but for the southeastern European region (26°E to 43°E, and 35°N to 43°N).

A.6.4 Blocks With/Without Heat

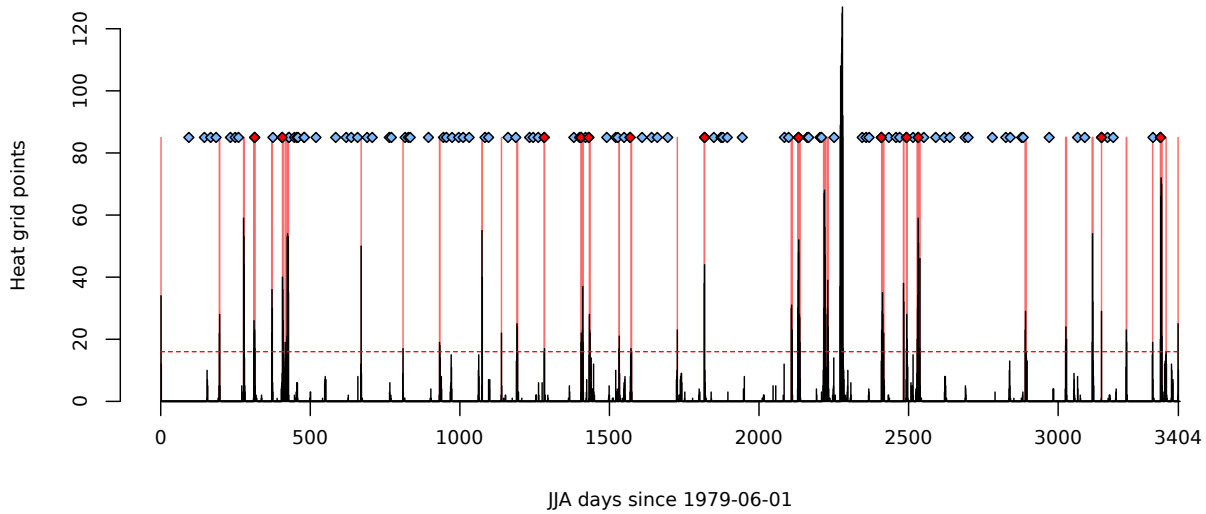

Figure A20: Same as Figure A12 but for the western European (WE) heat region (3°W to 13°, and 43° to 52°). The time step when a SCH10 block enters the block region (5° W to 15° E, and 50° N to 60° N) is marked with a rotated square. SCH10 blocks associated with WE heat days are shown as blue squares, SCH10 blocks not associated with WE heat days are shown as red squares.

A.6.5 Block Attributes

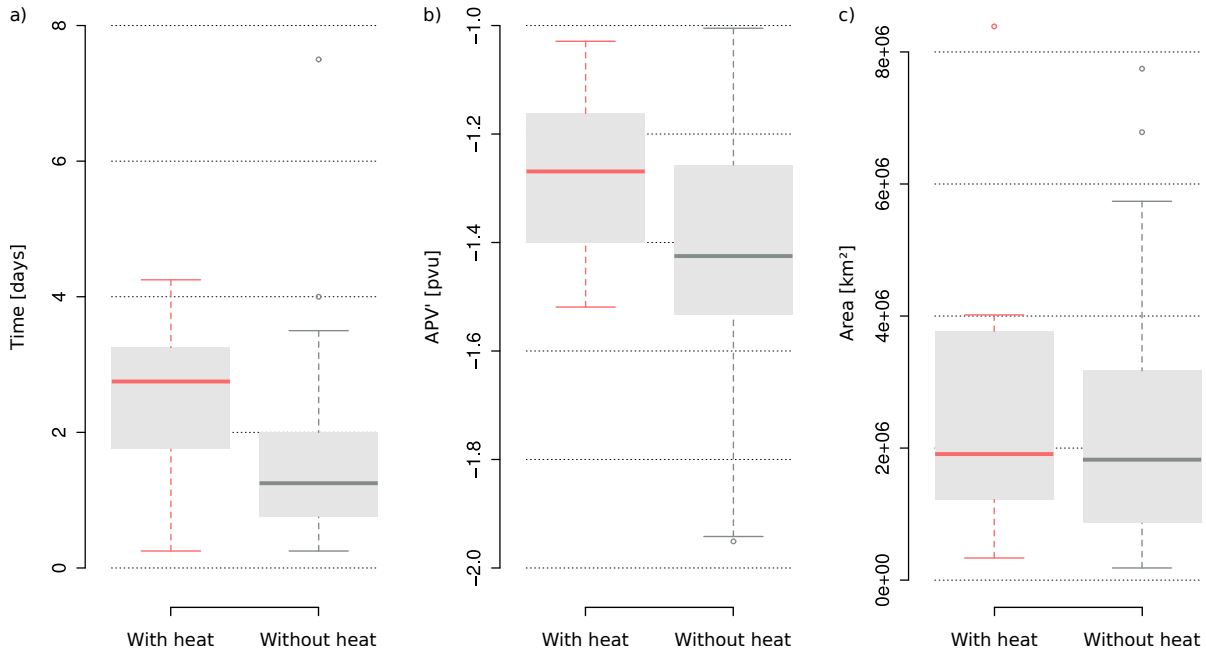

Figure A21: Shown is a) the time the SCH10 blocks are in the block region (5° W to 15° E, and 50° N to 60° N), b) the maximum area of the SCH10 blocks during their time in the block region, and c) the minimum APV' value of the SCH10 blocks during their time in the block region. The red boxplots are the SCH10 blocks with heat, the gray boxplots are the SCH10 blocks without heat. The boxplots show the median (thick horizontal line), the middle 50% of the data (gray box), the values 1.5 standard deviations away from the median (thin horizontal lines), and the outliers (circles).

Acronyms

APV	vertically-averaged potential vorticity
APV'	anomalous, vertically-averaged potential vorticity
DJF	December, January, February
EE	eastern Europe, eastern European
GPH	geopotential heigth
HD	heat day
HE	heat event
IB	Iberian Peninsula, Iberian
JJA	June, July, August
LGP	land grid point
MAM	March, April, May
NS	North Sea
RU	Russian, Russian
SC	Scandinavia, Scandinavian
SCH	SCHWIERZ et al. (2004) index
SCH07	SCHWIERZ et al. (2004) index with intensity threshold -0.7 pvu
SCH10	SCHWIERZ et al. (2004) index with intensity threshold -1.0 pvu
SCH13	SCHWIERZ et al. (2004) index with intensity threshold -1.3 pvu
SE	south-eastern Europe, south-eastern European
SON	September, October, November
TM2D	ROHRER et al. (2017) index
T2m	air temperature at two meters
OR	odds ratio
PV	potential vorticity
PV'	potential vorticity anomaly
RO200	ROHRER (2017a) index
WE	west Europe, western European
WSD	warm spell day
WSDI	warm spell day index

List of Figures

List of Tables

References

ALTENHOFF, A. M., O. MARTIUS, M. CROCI-MASPOLI, C. SCHWIERZ, and H. C. DAVIES (2008). Linkage of atmospheric blocks and synoptic-scale Rossby waves: a climatological analysis. *Tellus* **60A**: 1053–1063. DOI: 10.1111/j.1600-0870.2008.00354.x.

BARRIOPEDRO, D., R. GARCÍA-HERRERA, and R. M. TRIGO (2010). Application of blocking diagnosis methods to General Circulation Models. Part I: A novel detection scheme. *Climate Dynamics* **35**: 1373–1391. DOI: 10.1007/s00382-010-0767-5.

BIELI, M., S. PFAHL, and H. WERNLI (2015). A lagrangian investigation of hot and cold temperature extremes in europe. *Quarterly Journal of the Royal Meteorological Society* **141**: 98–108. DOI: 10.1002/qj.2339.

BLACK, E., M. BLACKBURN, R. G. HARRISON, B. J. HOSKINS, and J. METHVEN (2004). Factors contributing to the summer 2003 European heatwave. *Weather* **59**: 217–223. DOI: 10.1256/wea.74.04.

BLUESTEIN, H. B. (1993). *Synoptic-Dynamic Meteorology in Midlatitudes. Volume II: Observations and Theory of Weather Systems*. 1st edition. Oxford: University Press, 608pp. ISBN: 978-0-195062-68-7.

BRUNNER, L., G. C. HEGERL, and A. K. STEINER (2017). Connecting Atmospheric Blocking to European Temperature Extremes in Spring. *Journal of Climate* **30**: 585–594. DOI: 10.1175/JCLI-D-16-0518.1.

BUEHLER, T., C. C. RAIBLE, and T. F. STOCKER (2011). The relationship of winter season North Atlantic blocking frequencies to extreme cold or dry spells in the ERA-40. *Tellus, Series A: Dynamic Meteorology and Oceanography* **63**: 212–222. DOI: 10.1111/j.1600-0870.2010.00492.x.

CHANG, E. K. M., S. LEE, and K. L. SWANSON (2002). Storm track dynamics. *Journal of Climate* **15**: 2163–2183. DOI: 10.1175/1520-0442(2002)015<02163:STD>2.0.CO;2.

DEE, D. P., S. M. UPPALA, A. J. SIMMONS, P. BERRISFORD, P. POLI, S. KOBAYASHI, U. ANDRAE, M. A. BALMASEDA, G. BALSAMO, P. BAUER, P. BECHTOLD, A. C. M. BELJAARS, L. VAN DE

BERG, J. BIDLOT, N. BORMANN, C. DELSOL, R. DRAGANI, M. FUENTES, A. J. GEER, L. HAIMBERGER, S. B. HEALY, H. HERSBACH, E. V. HÓLM, L. ISAKSEN, P. KÅLLBERG, M. KÖHLER, M. MATRICARDI, A. P. MCNALLY, B. M. MONGE-SANZ, J. J. MORCRETTE, B. K. PARK, C. PEUBEY, P. DE ROSNAY, C. TAVOLATO, J. N. THÉPAUT, and F. VITART (2011). The ERA-Interim reanalysis: Configuration and performance of the data assimilation system. *Quarterly Journal of the Royal Meteorological Society* **137**: 553–597. DOI: 10.1002/qj.828.

DOLE, R. M. and N. D. GORDON (1983). Persistent anomalies of the extratropical Northern Hemisphere wintertime circulation - Structure. *Monthly Weather Review* **111**: 1567–1586. DOI: 10.1175/1520-0493(1983)111<1567:PAOTEN>2.0.CO;2.

DOLE, R., M. HOERLING, J. PERLWITZ, J. EISCHEID, P. PEGION, T. ZHANG, X. W. QUAN, T. XU, and D. MURRAY (2011). Was there a basis for anticipating the 2010 Russian heat wave? *Geophysical Research Letters* **38**: 1–5. DOI: 10.1029/2010GL046582.

ELLIOTT, R. D. and T. B. SMITH (1949). A Study of the Effects of Large Blocking Highs on the General Circulation in the Northern-Hemisphere Westerlies. *Journal of Meteorology* **6**: 68–85. DOI: 10.1175/1520-0469(1949)006<0068:ASOTEO>2.0.CO;2.

FISCHER, E. M., S. I. SENEVIRATNE, D. LÜTHI, and C. SCHÄR (2007). Contribution of land-atmosphere coupling to recent European summer heat waves. *Geophysical Research Letters* **34**: 1–6. DOI: 10.1029/2006GL029068.

FREDERIKSEN, J. S. (1982). A Unified Three-Dimensional Instability Theory of the Onset of Blocking and Cyclogenesis. *Journal of the Atmospheric Sciences* **39**: 969–982. DOI: 10.1175/1520-0469(1983)040<2593:AUTDIT>2.0.CO;2.

GARCÍA-HERRERA, R., R. M. TRIGO, J. LUTERBACHER, and E. M. FISCHER (2010). A Review of the European Summer Heat Wave of 2003. *Critical Reviews in Environmental Science and Technology* **40**: 267–306. DOI: 10.1080/10643380802238137.

GOVERNMENT OF CANADA (2017a). *Environment and Climate Change*. URL: http://ec.gc.ca/meteo-weather/default.asp?lang=En%7B%5C&%7Dn=04A1BF3B-1 (visited on 04/23/2017).

GOVERNMENT OF CANADA (2017b). *Glossary Climate and Weather*. URL: http://climate.weather.gc.ca/glossary%7B%5C_%7De.html (visited on 01/13/2017).

HOSKINS, B. J. (1987). *Theories of blocking*. Conference Paper. Seminar on the Nature and Prediction of Extra Tropical Weather Systems. 7-11 September 1987. Shinfield Park, Reading.

HOSKINS, B. J. (1985). On the use and significance of isentropic potential vorticity maps. *Quarterly Journal of the Royal Meteorological Society* **111**: 877–946. DOI: 10.1002/qj.49711147002.

KOTRONI, V., K. LAGOUVARDOS, and A. RETALIS (2011). The heat wave of June 2007 in Athens, Greece - Part 2: Modeling study and sensitivity experiments. *Atmospheric Research* **100**: 1–11. DOI: 10.1016/j.atmosres.2010.12.007.

LAU, W. K. M. and K.-M. KIM (2012). The 2010 Pakistan Flood and Russian Heat Wave: Teleconnection of Hydrometeorological Extremes. *Journal of Hydrometeorology* **13**: 392–403. DOI: 10.1175/JHM-D-11-016.1.

LEJENÄS, H. and H. ØKLAND (1983). Characteristics of northern hemisphere blocking as determined from a long time series of observational data. *Tellus A* **35**: 350–362. DOI: 10.3402/tellusa.v35i5.11446.

MALGUZZI, P. and P. MALANOTTE-RIZZOLI (1984). Nonlinear Stationary Rossby Waves on Nonuniform Zonal Winds and Atmospheric Blocking. Part I: The Analytical Theory. *Journal of the Atmospheric Sciences* **41**: 2620–2628. DOI: 10.1175/1520-0469(1984)041<2620:NSRWON>2.0.CO;2.

MARTIN, J. E. (2006). *Mid-latitude atmospheric dynamics*. Chichester: Wiley, 324pp. ISBN: 13 978-0-470-86464-7.

MEEHL, G. A. and C. TEBALDI (2004). More Intense, More Frequent, and Longer Lasting Heat Waves in the 21st Century. *Science* **305**: 994–997. DOI: 10.1126/science.1098704.

METÉIREANN (2013). *Monthly Weather Bulletin July 2013.* Dublin: MetÉireann, 16pp.

METEOSCHWEIZ (2016). *Der Hitzesommer 2015 in der Schweiz*. Zürich: Bundesamt für Meteorologie und Klimatologie, 68pp.

METOFFICE (2016). *July 2013 heat wave*. URL: http://www.metoffice.gov.uk/learning/learn-about-the-weather/weather-phenomena/case-studies/heat-wave-july2013 (visited on 12/14/2016).

PELLY, J. L. and B. J. HOSKINS (2003). A New Perspective on Blocking. *Journal of the Atmospheric Sciences* **60**: 743–755. DOI: 10.1175/1520-0469(2003)060<0743:ANPOB>2.0.CO;2.

PELLY, J. L. (2001). *The predictability of atmospheric blocking*. Dissertation. The University of Reading, 207pp.

PERKINS, S. E. (2015). A review on the scientific understanding of heatwaves - Their measurement, driving mechanisms, and changes at the global scale. *Atmospheric Research* **164-165**: 242–267. DOI: 10.1016/j.atmosres.2015.05.014.

PFAHL, S., C. SCHWIERZ, M. CROCI-MASPOLI, C. M. GRAMS, and H. WERNLI (2015). Importance of latent heat release in ascending air streams for atmospheric blocking. *Nature Geoscience* **8**: 610–614. DOI: 10.1038/ngeo2487.

PFAHL, S. and H. WERNLI (2012). Quantifying the relevance of atmospheric blocking for co-located temperature extremes in the Northern Hemisphere on (sub-)daily time scales. *Geophysical Research Letters* **39**: 1–6. DOI: 10.1029/2012GL052261.

REBETEZ, M., O. DUPONT, and M. GIROUD (2009). An analysis of the July 2006 heatwave extent in Europe compared to the record year of 2003. *Theoretical and Applied Climatology* **95**: 1–7. DOI: 10.1007/s00704-007-0370-9.

REX, D. F. (1950). Blocking Action in the Middle Troposphere and its Effect upon Regional Climate: II. The Climatology of Blocking Action. *Tellus* **2**: 275–301. DOI: 10.1111/j.2153-3490.1950.tb00339.x.

ROBINE, J. M., S. L. K. CHEUNG, S. LE ROY, H. VAN OYEN, C. GRIFFITHS, J. P. MICHEL, and F. R. HERRMANN (2008). Death toll exceeded 70,000 in Europe during the summer of 2003. *Comptes Rendus - Biologies* **331**: 171–178. DOI: 10.1016/j.crvi.2007.12.001.

ROHRER, M. (2017a). Personal communication.

ROHRER, M. (2017b). *Long-term changes of weather extremes in a large ensemble of climate model simulations*. Dissertation. Universität Bern, 257pp.

ROHRER, M., S. BRÖNNIMANN, O. MARTIUS, C. C. RAIBLE, M. WILD, and G. P. COMPO (2017). Representation of extratropical cyclones, blocking anticyclones, and circulation types in multiple reanalyses and model simulations. *Submitted to Journal of Climate*.

RUSSO, S., A. F. MARCHESE, J. SILLMANN, R. VAUTARD, A. GOBIET, S. SOBOLOWSKI, L. J. HARRINGTON, D. J. FRAME, E. M. FISCHER, S. RUSSO, J. SILLMANN, and E. M. FISCHER (2015). Top ten European heatwaves since 1950 and their occurrence in the coming decades. *Environmental Research Letters* **10**: 124003. DOI: 10.1088/1748-9326/10/12/124003.

SCHERRER, S. C., M. CROCI-MASPOLI, C. SCHWIERZ, and C. APPENZELLER (2006). Two- dimensional indices of atmospheric blocking and their statistical relationship with winter climate patterns in the Euro-Atlantic region. *International Journal of Climatology* **26**: 233–249. DOI: 10.1002/joc.1250.

SCHNEIDEREIT, A., S. SCHUBERT, P. VARGIN, F. LUNKEIT, X. ZHU, D. H. W. PETERS, and K. FRAEDRICH (2012). Large-Scale Flow and the Long-Lasting Blocking High over Russia : Summer 2010. *Monthly Weather Review* **140**: 2967–2981. DOI: 10.1175/MWR-D-11-00249.1.

SCHWIERZ, C., M. CROCI-MASPOLI, and H. C. DAVIES (2004). Perspicacious indicators of atmospheric blocking. *Geophysical Research Letters* **31**: L06125. DOI: 10.1029/2003GL019341.

SHUTTS, G. J. (1983). The propagation of eddies in diffluent jetstreams: Eddy vorticity forcing of 'blocking' flow fields. *Quarterly Journal of the Royal Meteorological Society* **109**: 737–761. DOI: 10.1002/qj.49710946204.

SILLMANN, J., C. M. MISCHA, M. KALLACHE, and R. W. KATZ (2011). Extreme cold winter temperatures in Europe under the influence of North Atlantic atmospheric blocking. *Journal of Climate* **24**: 5899–5913. DOI: 10.1175/2011JCLI4075.1.

SOUSA, P. M., D. BARRIOPEDRO, R. M. TRIGO, A. M. RAMOS, R. NIETO, L. GIMENO, K. F. TURKMAN, and M. L. R. LIBERATO (2016). Impact of Euro-Atlantic blocking patterns in iberia precipitation using a novel high resolution dataset. *Climate Dynamics* **46**: 2573–2591. DOI: 10.1007/s00382-015-2718-7.

SOUSA, P. M., R. M. TRIGO, D. BARRIOPEDRO, P. M. M. SOARES, and J. A. SANTOS (2017). European temperature responses to blocking and ridge regional patterns. *Climate Dynamics*, 1–21. DOI: 10.1007/s00382-017-3620-2.

STEFANON, M., F. D'ANDREA, and P. DROBINSKI (2012). Heatwave classification over Europe and the Mediterranean region. *Environmental Research Letters* **7**: 014023. DOI: 10.1088/1748-9326/7/1/014023.

TIBALDI, S. and F. MOLTENI (1990). On the operational predictability of blocking. *Tellus A* **42**: 343–365. DOI: 10.1034/j.1600-0870.1990.t01-2-00003.x.

TREIDL, R., E. BIRCH, and P. SAJECKI (1981). Blocking action in the northern hemisphere: A Climatological study. *Atmosphere-Ocean* **19**: 1–23. DOI: 10.1080/07055900.1981.9649096.

TRIGO, R. M., I. F. TRIGO, C. C. DACAMARA, and T. J. OSBORN (2004). Climate impact of the European winter blocking episodes from the NCEP/NCAR reanalyses. *Climate Dynamics* **23**: 17–28. DOI: 10.1007/s00382-004-0410-4.

TRIGO, R. M., R. GARCÍA-HERRERA, J. DÍAZ, I. F. TRIGO, and M. A. VALENTE (2005). How exceptional was the early August 2003 heatwave in France? *Geophysical Research Letters* **32**: 1–4. DOI: 10.1029/2005GL022410.

WALLACE, J. M. and P. V. HOBBS (2006). *Atmospheric Science: An Introductory Survey.* Edited by R. DMOWSKA, D. HARTMANN, and H. ROSSBY. 2nd edition. Amsterdam: Elsevier, 483pp. ISBN: 978-0-127329-51-2.

YAMADA, T. J., D. TAKEUCHI, M. A. FARUKH, and Y. KITANO (2016). Climatological characteristics of heavy rainfall in northern Pakistan and atmospheric blocking over western Russia. *Journal of Climate* **29**: 7743–7754. DOI: 10.1175/JCLI-D-15-0445.1.

Z'GRAGGEN, L. (2006). *Die Maximaltemperaturen im Hitzesommer 2003 und Vergleich zu früheren Extremtemperaturen*. Zürich: Bundesamt für Meteorologie und Klimatologie, 78pp.

Acknowledgements

My gratitude goes to Olivia Martius-Romppainen, Sina Lenggenhager, and Matthias Röthlisberger for taking time to answer my questions, giving me valuable ideas and literature hints, preparing data, and providing instructive feedback. I also would like to thank Marco Rohrer and Andrey Martinov for the help with various computer issues, and especially Marco Rohrer for providing the code of the blocking indices.

Another thank you goes to all my workmates at the GIUB who contributed to a nice working atmosphere and many interesting coffee breaks. Further I would like to thank Kim Hays for improving my English writing, and making this text more enjoyable to read. A big thank you goes to my flatmates Annina, Rahel, and Karin for all the encouraging words regarding my work, to my cousin Sibylle for the time we spent together writing our Master's theses, and to Samir for exactly knowing how to motivate me. Moreover, I would like to express my thanks to my parents Christine and Peter who in the first place enabled my studies and always showed a lot of interest in what I am doing.

Last but not least I thank all the people who simplified my work by making sure that tools like NCL, CDO, R studio, and Inkscape are open-source, and ECMWF for producing and providing the ERA-interim data freely.

Declaration

under Art. 28 Para. 2 RSL 05

Last, first name: Villiger, Leonie

Matriculation number: 11-109-188

Programme: Master of Science in Climate Sciences with special qualification in Atmospheric Science

Bachelor ☐ Master ☐ Dissertation ☐

Thesis title: Block detection and European heat waves

Thesis supervisor: Prof. Dr. Olivia Romppainen-Martius

I hereby declare that this submission is my own work and that, to the best of my knowledge and belief, it contains no material previously published or written by another person, except where due acknowledgement has been made in the text. In accordance with academic rules and ethical conduct, I have fully cited and referenced all material and results that are not original to this work. I am well aware of the fact that, on the basis of Article 36 Paragraph 1 Letter o of the University Law of 5 September 1996, the Senate is entitled to deny the title awarded on the basis of this work if proven otherwise. I grant inspection of my thesis.

.....

Place, date

.....

Signature